



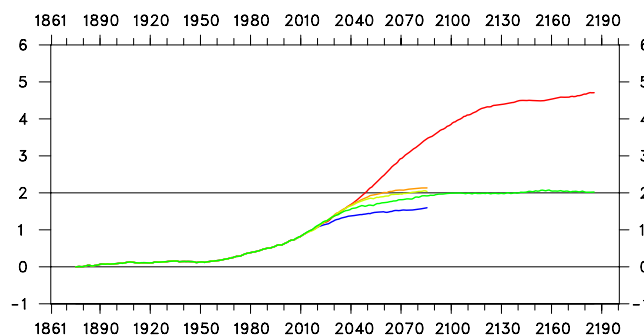
## Danish Climate Centre Report 06-03

# Towards a global "2 degree C-stabilization" scenario: estimates of the allowable greenhouse gas concentrations and the associated climatic changes

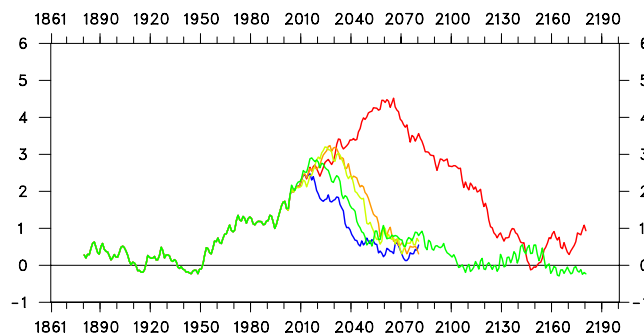
Wilhelm May

### Near-surface temperature

#### Anomaly



#### Change rate





# Colophon

**Serial title:**

Danish Climate Centre Report 06-03

**Title:**

Towards a global "2 degree C-stabilization" scenario: estimates of the allowable greenhouse gas concentrations and the associated climatic changes

**Subtitle:**

**Author(s):**

Wilhelm May

**Other contributors:**

**Responsible institution:**

Danish Meteorological Institute

**Language:**

English

**Keywords:**

**Url:**

[www.dmi.dk/dmi/dkc06-03](http://www.dmi.dk/dmi/dkc06-03)

**ISBN:**

87-8478-543-5

**ISSN:**

1399-1957

**Version:**

**Website:**

[www.dmi.dk](http://www.dmi.dk)

**Copyright:**



## Content:

Abstract .....	4
1. Introduction.....	4
2. Model and experimental design .....	5
2.1 Model description .....	5
2.2 Model experiments.....	6
3. Global mean changes .....	7
3.1 Near-surface temperature .....	8
3.2 Precipitation .....	9
3.3 Sea-ice conditions .....	10
4. Zonal mean changes.....	12
4.1 Near-surface variables.....	12
4.2 Latitude-height cross sections .....	14
5. Local changes.....	16
5.1 Sea-ice conditions .....	16
5.2 Near-surface temperature .....	19
5.3 Precipitation .....	20
5.4 Sea-level pressure .....	22
5.5 Root-mean-square differences .....	23
6. Summary and conclusions .....	24
Acknowledgements.....	27
References.....	28
Previous reports.....	29

## Abstract

The atmospheric greenhouse gas concentrations for keeping the future global warming at 2 °C relative to pre-industrial levels are specified. Furthermore, the projected changes in various meteorological and oceanic variables associated with this particular scenario are described.

## 1. Introduction

The objective of Article 2 of the United Nations Framework Convention on Climate Change (UNFCCC) formulated in 1992 is “to achieve stabilization of greenhouse gas concentrations in the atmosphere that would prevent dangerous anthropogenic interference with the climate system” (United Nations 1992). The convention further suggests that “such a level should be achieved within a time frame sufficient to allow ecosystems to adapt naturally to climate change, to ensure that food production is not threatened, and to enable economic development to proceed in a sustainable manner”. In the European Union, the Council of Environment Ministers laid down in a statement dated October 17, 2002, that in order to obtain this objective “global efforts should be guided by a long-term objective of a global temperature increase of 2 °C over pre-industrial levels and a stabilization of CO<sub>2</sub> concentrations below 550 ppm.”. This so-called “EU-target” has since then been reaffirmed by the EU on a number of occasions.

But even a global mean temperature increase of 2 °C can have adverse effects, even at large scales. The loss of the Greenland ice sheet, for instance, may be triggered by a local temperature increase of approximately 2.7° (Huybrechts et al. 1991, Gregory et al. 2004), possibly corresponding to a global mean temperature increase of less than 2 °C. This loss is likely to cause a global sea-level rise of 7 m over the next 1000 years or more (Gregory et al. 2004). Unique ecosystems such as corral reefs and ecosystems in the Arctic or the Alpine region are increasingly under pressure and may be severely damaged by a global mean temperature increase of 2 °C and below (e.g., Smith et al. 2001, ACIA 2005). In addition, strong positive feedbacks with the carbon cycle are increasingly likely (e.g., Friedlingstein et al. 2003, Jones et al. 2003a, b), amplifying climate change beyond the direct effects of the anthropogenic emissions. Similarly, potentially large but very uncertain methane releases might occur from thawing permafrost or ocean methane hydrates (Archer et al. 2004, Buffet and Archer 2004).

In February 2005 an international symposium on “Avoiding Dangerous Climate Change” took place in Exeter, UK. Important issues of “dangerous” climate change were addressed, such as vulnerabilities of the climate system (and critical thresholds), vulnerabilities for ecosystems and biodiversity, and vulnerabilities for water resources, agriculture and food as well as climate change impacts in various sensitive regions of the globe (Schellnhuber et al. 2006). Also, possible emission pathways to reach stabilization of the greenhouse gas concentrations at a level that could prevent dangerous climate change were discussed as well as technological options to realize these pathways.

Meinshausen (2006) addressed, for instance, the question of how low the greenhouse gas concentrations need to peak or stabilize at for not exceeding the EU-target of a maximum global mean temperature increase of 2 °C. On the basis of a number of published climate sensitivities, he concluded that the probability for staying below a warming of 2 °C at equilibrium is “likely” or “very likely” (according to the IPCC terminology of probabilities) at 400 ppm equivalent CO<sub>2</sub>, while at 475 ppm the probability is at “medium likelihood” or “unlikely”. At 550 ppm equivalent CO<sub>2</sub>, on the other hand, the risk of overshooting the EU-target is 63% and, assuming a climate sensitivity range consistent with the conventional range of 1.5-4.5 °C used by the IPCC (Wigley and Raper 2001), the risk of overshooting 4 °C as the global mean temperature increase is still 9%. It was also found that if the equivalent CO<sub>2</sub> concentration temporarily overshoot the 400 ppm stabilization level by 75 ppm, the probability of keeping the future warming below 2 °C decreased by 10-20%, depending on

the rate at which the greenhouse gas concentrations were reduced after the peaking. However, the overshooting of such low stabilization levels might be necessary, given that a peaking at 475 ppm equivalent CO<sub>2</sub> is already asking for substantial emission reductions in the coming two to three decades.

Den Elzen and Meinshausen (2006) analyzed possible emission pathways including several greenhouse gases as well as the effects of aerosols for meeting the EU-target. They found that in order to reach the 400 ppm equivalent CO<sub>2</sub> stabilization level proposed by Meinshausen (2006) the global emissions are required to peak around 2015 in order to avoid global reduction rates exceeding 2.5%/yr, followed by substantial reductions by as much as 40-45% in 2050 compared to the levels in 1990. Brasseur and Roeckner (2005), investigating the impact of improved air quality on the future evolution of climate, found that the stabilization of aerosol loads is so important that it has to be considered in strategies aiming to maintain the global warming below a certain threshold.

So far there have not been any studies investigating the impacts of a global mean temperature increase of 2 °C (or any other prescribed threshold) on the climate system by using a complex coupled climate model. This would, however, be necessary in order to evaluate how strongly the EU-target affects certain aspects of climate and how big an improvement this means relative to stronger emission scenarios, such as the A1, A2 or B2 families of scenarios proposed by the IPCC (Nakićenović et al. 2000). Therefore, in this study a particular scenario for keeping the future warming at 2 °C with respect to pre-industrial times is specified, using the ECHAM5/MPI-OM coupled climate model. This scenario considers atmospheric greenhouse gas concentrations and anthropogenic aerosol emissions as well as ozone levels throughout the atmosphere. Although the characteristics of this scenario to some extent depend on the characteristics of the model, i.e., on its climate sensitivity, the study gives an essential idea about the point in time at which the greenhouse gas concentrations have to be kept constant in order to avoid dangerous climate change. The projected changes in various meteorological and oceanic variables associated with this so-called “2 °C-stabilization” scenario are presented and compared to the respective changes associated with the SRES A1B scenario used in the upcoming IPCC-report. Furthermore, the role of the anthropogenic aerosol emissions for defining the stabilization scenario and their impact on the simulated future climate are investigated.

The report is organized as follows: The coupled climate model and the different model experiments used in this study are introduced in Section 2. In the following sections the simulated changes in various meteorological and oceanic variables are discussed, i.e., the global mean changes in Section 3, the zonal mean changes in Section 4 and the local changes in Section 5, respectively. A summary and the conclusions are given in Section 6.

## 2. Model and experimental design

### 2.1 Model description

The model used is the Hamburg coupled atmosphere-ocean model, combining the ECHAM5 atmospheric general circulation model (“AGCM”; Roeckner et al. 2003, 2006) and the MPI-OM ocean/sea-ice model (Marsland et al. 2003). ECHAM5 uses the spectral transform method for vorticity, divergence and the logarithm of surface pressure at T63 horizontal resolution with 31 levels in a hybrid sigma/pressure coordinate system in the vertical with the top level at 10 hPa. It uses state-of-the-art parameterizations for shortwave and longwave radiation, stratiform clouds, boundary layer and land-surface processes, and gravity wave drag. The direct aerosol effect is calculated by transforming the prescribed sulphate mass into number concentrations assuming a log-normal size distribution and considering the dependence of particle size on ambient relative humidity (Hess et al. 1998). The first indirect effect is included via empirical relationships between sulphate mass and the cloud droplet

number concentration (Boucher and Lohmann 1995).

MPI-OM employs the primitive equations for a hydrostatic Boussinesq fluid with a free surface at a resolution of  $1.5^\circ$  and a vertical discretization at 40 z-levels. The poles of the curvilinear grid are shifted to land areas over Greenland and Antarctica. Parameterized processes include along-isopycnal diffusion, horizontal tracer mixing by advection with unresolved eddies, vertical eddy mixing, near-surface wind stirring, convective overturning, and slope convection. Concentration and thickness of sea-ice are simulated by a dynamic and thermodynamic sea-ice model. In the coupled model (Jungclaus et al. 2006), the ocean passes to the atmosphere the sea-surface temperature, sea-ice concentration and thickness, snow depth on ice, and ocean surface velocities. Using these boundary values, the AGCM accumulates the forcing fluxes (wind stress, heat, freshwater including river runoff and glacier calving, and 10 m wind speed) during the coupling time step of one day and passes the daily mean fluxes to the ocean model. All fluxes are calculated separately for ice-covered and open water partitions of the grid cells.

## 2.2 Model experiments

The ECHAM5/MPI-OM coupled model has been used for several simulations with varying concentrations of well-mixed greenhouse gases, i.e.,  $\text{CO}_2$ ,  $\text{CH}_4$ ,  $\text{N}_2\text{O}$ , CFC-11 (including a small contribution from natural sources), and CFC-12, ozone ( $\text{O}_3$ ), and sulphate aerosols ( $\text{SO}_4$ ) prescribed. In one simulation over the period 1861-2200, the concentrations of these substances have been prescribed according to observations until 2000 and according to the SRES A1B scenario (Nakićenović et al. 2000) for the period 2001-2100. After 2100 all concentrations have been kept constant at the level of 2100. This simulation (referred to as “A1B” in the following; see Table 1) shows a warming of  $3.47^\circ\text{C}$  by the end of the 21<sup>st</sup> century and of about  $4.71^\circ\text{C}$  by the end of the 22<sup>nd</sup> century due to the prescribed anthropogenic changes in the greenhouse gas concentrations (see Table 2).

Experiment	Period	$\text{CO}_2$ , $\text{CH}_4$ , $\text{N}_2\text{O}$ , CFC-11, and CFC-12	$\text{O}_3$ and $\text{SO}_4$
A1B	1861-2200	Observations (1861-2000) A1B scenario (2001-2100) A1B level for 2100 (2101-2200)	Observations (1861-2000) A1B scenario (2001-2100) A1B level for 2100 (2101-2200)
2C20	2020-2200	A1B level for 2020	A1B scenario* (2020-2036) A1B level 2100 (2037-2200)
2C25	2025-2100	A1B level for 2025	A1B scenario* (2025-2040) A1B level 2100 (2041-2100)
2C30	2030-2100	A1B level for 2030	A1B scenario* (2030-2044) A1B level 2100 (2045-2100)
2C30A	2030-2100	A1B level for 2030	A1B level for 2030

**Table 1:** List of experiments; \* this scenario approaches the level for 2100 5 times faster than for the original A1B scenario

The primary goal of the experiments was to construct a scenario close to a global mean temperature change of  $2^\circ\text{C}$  with respect to the pre-industrial period 1861-1890 by the end of the 21<sup>st</sup> century without exceeding this threshold. It could, however, happen that the warming exceeds this threshold at a later stage since the coupled model presumably has not reached its equilibrium at the end of the 21<sup>st</sup> century. A1B shows a warming of  $0.97^\circ\text{C}$  for the period 2001-2030 and an additional unreal-

ized warming of 1.24 °C between the periods 2071-2100 and 2171-2200, i.e., over the period with constant concentrations of the various greenhouse gases. Assuming a weaker additional warming at an earlier time, one could expect a warming of 2 °C by the end of the 21<sup>st</sup> century when starting the simulation in 2030 with starting conditions from A1B, keeping the greenhouse gas concentrations at the level of 2030 and ozone and sulphate at the level of 2100. The level of equivalent CO<sub>2</sub> for 2030 is 533.6 ppm, compared to 305.0 ppm and 877.4 ppm for 1890 and 2100, respectively. In this simulation (“2C30”), the levels of ozone and sulphate change 5 times as fast as in A1B, reaching the level for 2100 after 15 years. But the simulation exceeds the 2 °C threshold by the end of the 21<sup>st</sup> by 0.13 °C (see Table 2), so that another simulation was started in 2025 with a weaker warming of 0.84 °C. But also this simulation (“2C25”) exceeds the 2 °C threshold by 0.04 °C, making a third simulation (“2C20”) necessary to be started in 2020 with a warming of 0.73 °C and an equivalent CO<sub>2</sub> level of 488.6 ppm. The atmospheric concentrations of the main greenhouse gases for 2020 are 418 ppm (CO<sub>2</sub>), 2026 ppb (CH<sub>4</sub>), and 331 ppb (N<sub>2</sub>O), respectively. This simulation reveals a warming of 1.92 °C by the end of the 21<sup>st</sup> century.

Experiment	Period 2071-2100	Period 2171-2200
A1B	3.47	4.71
2C20	1.92	2.02
2C20M	1.88	2.06
2C25	2.04	
2C30	2.13	
2C30A	1.60	

**Table 2:** Change in global annual mean near-surface temperature for two periods with respect to the period 1861-1890 (14.03 °C).

In order to evaluate the dependency on the particular scenario for the aerosols and the ozone concentrations, an additional simulation (“2C30A”) was performed that like 2C30 started in 2030 with the greenhouse gas concentrations at the level of 2030 but also with ozone and sulphate at the level of 2030 according to the A1B scenario. The SO<sub>2</sub> emissions, for instance, are 72% stronger in 2030 than in 2100 with about 92 TgS/yr and 26 TgS/yr, respectively (Nakićenović et al. 2000). The ozone concentrations, on the other hand, are somewhat lower for 2030 than for 2100. In the middle stratosphere (150 hPa), for instance, the average concentrations are about 25% higher than in 2100. The higher aerosol emissions and weaker ozone concentrations in 2C30A lead to a weaker warming of 1.60 °C by the end of the 21<sup>st</sup> century compared to 2.13 °C for 2C30 (see Table 2).

### 3. Global mean changes

In this section, time series of the annual mean changes in the global mean temperature and daily precipitation as well as of the semi-annual mean changes in the sea-ice extent and sea-ice volume in

the Arctic and the Antarctic region, respectively, are considered.

### 3.1 Near-surface temperature

A1B shows a continuous warming relative to pre-industrial times throughout almost the entire period 1861-2200, with 3.47 °C by the end of the 21<sup>st</sup> century and 4.71 °C by the end of the 22<sup>nd</sup> century (Fig. 1a). This is a warming of 3.13 °C relative to the period 1961-1990, which is somewhat higher than the average warming of 2.50 °C but well within the range of 1.20-3.70 °C presented in the 3<sup>rd</sup> IPCC report for the A1B scenario (Cubasch et al. 2001). The strongest warming rate of more than 4.5 °C/century occurs around 2060 (Fig. 1b), in response to both a strong increase in all greenhouse gas concentrations except CH<sub>4</sub> and a marked decrease in the SO<sub>2</sub> emissions (Nakićenović et al. 2000). After the concentrations of the greenhouse gases and aerosols are kept constant at the level of 2100, the warming continues throughout the rest of the simulation, particularly during the first 30 years with more than 1 °C/century.

#### Near-surface temperature

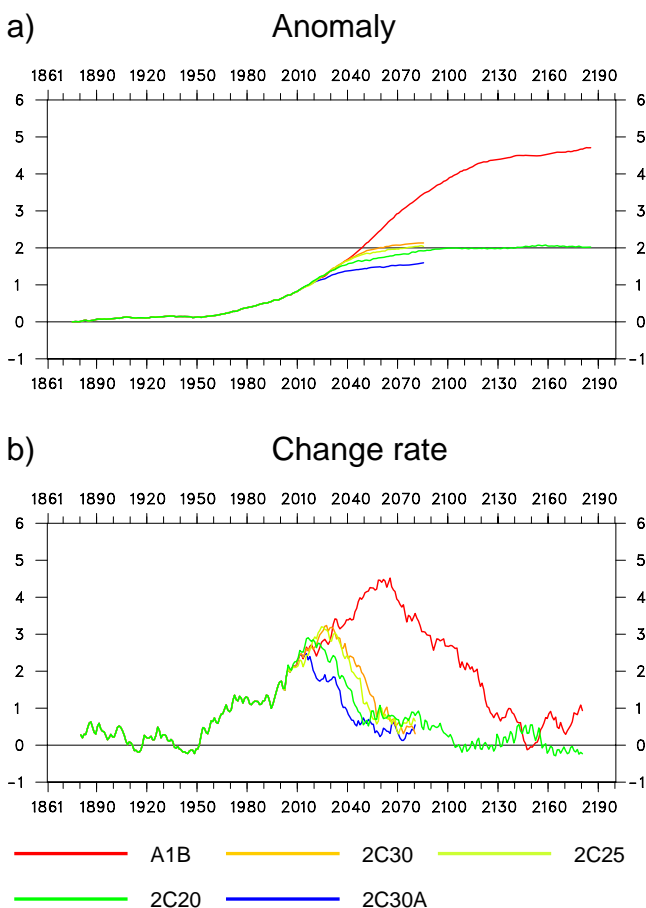


**Figure 1:** Changes in the 30-year averages of global annual mean near-surface temperature with respect to the period 1861-1890 (14.03 °C) (a) and 10-year running means of the year-to-year differences of these 30-year averages (b) for the different experiments. Units are [°C] (a) and [°C/century] (b). The years indicate the centres of the 30-year periods.

For the other experiments, the strongest warming rates reach only between 2.5 and 3.5 °C/century shortly after the greenhouse gas concentrations are kept constant (Fig. 1b). A small portion of the warming is due to the decreasing aerosol emissions and increasing ozone concentrations over the first 15 to 17 years of the simulations. After reaching the maximum, the warming rates decrease

over the following 30 years and stay at about 1 °C/century thereafter. For 2C20, the warming rate eventually (around 2100) varies around 0 °C/century, indicating that this simulation has reached its equilibrium. This illustrates that the rate at which the climate simulation reaches its equilibrium and, hence, the magnitude of the unrealized warming, strongly depends on the magnitude of the warming. The latter, in turn, is determined by the strength of the greenhouse gas forcing. Starting from 0.73 °C in 2020, 2C20 stays below a warming of 2 °C until the mid of the 22<sup>nd</sup> century, reaching a maximum warming of 2.07 °C a few decades later (Fig. 1a). After the stabilization of the simulated climate, the warming is stronger over the land areas (2.80 °C) than over the oceans (1.80 °C).

For 2C30A, on the other hand, the warming rate below 1 °C/century is reached about 20 years earlier than for 2C30 (around 2040 vs. 2060; Fig. 1b), again illustrating how important the magnitude of the warming is for the stabilization rate. The higher aerosol emissions and the lower ozone concentrations in 2C30A, lead to a relatively weak warming in this experiment with 1.60 °C by the end of the 21<sup>st</sup> century, which is 0.53 °C less than for 2C30. The higher aerosol emissions lead to a marked cooling, which can be attributed to both the direct and the indirect radiative effect of the sulphate aerosols (Brasseur and Roeckner 2005). When totally removing the anthropogenic sulphate aerosols from the atmosphere, Brasseur and Roeckner (2005) found an additional warming of 0.80 °C for the year 2000 due to the improved air quality. With ozone being a greenhouse gas, also the lower ozone concentrations contribute to the weaker warming in 2C30A.

## 3.2 Precipitation

Similar to the near-surface temperature, the simulated changes in the global annual mean daily precipitation show a continuous increase throughout almost the entire period (Fig. 2a). The increases reach 0.18 mm/d for A1B and 0.10 mm/d for 2C20 by the end of the 21<sup>st</sup>, and 0.26 mm/d (A1B) and 0.12 mm/d (2C20) by the end of the 22<sup>nd</sup> century. The latter numbers correspond to an increase of 8.9 and 4.1%, respectively, relative to pre-industrial times. Relative to the period 1961-1990, A1B gives an increase in daily precipitation of 6.1 % by the end of the 21<sup>st</sup> century and 2C20 an increase by 3.3%. The precipitation change simulated in A1B is larger than the mean precipitation changes reported in the 3<sup>rd</sup> IPCC-report with 3.9% for the A2 and 3.3% for the B2 scenario (Cubasch et al. 2001), but still within the upper range of 6.8% for the A2 scenario. The two simulations starting at 2030 show increases of 0.07 mm/d (2C30A) and 0.12 mm/d (2C30), respectively, illustrating a weaker increase in daily precipitation associated with the weaker warming. This is, again, consistent with the results by Brasseur and Roeckner (2005), who found an increase of the globally averaged precipitation by 3% as a consequence of the removal of the anthropogenic sulphate aerosols. They suggested that the changes in precipitation were largely driven by the temperature changes in response to the removal of the aerosols.

It is interesting to note that in the beginning of the three experiments with the constant levels of greenhouse gases and the rapidly decreasing aerosol emissions (2C20, 2C25, and 2C30) the increase in daily precipitation is markedly stronger than in A1B with increasing aerosol emissions, while for the near-surface temperature these differences are negligible (see Fig. 1a). Apparently, the rapid decrease in the aerosol concentrations leads to a fast increase in daily precipitation, while the associated additional warming evolves less rapidly.

A1B shows the strongest change rate (about 0.3 mm/d/century) around 2060 (Fig. 2b), corresponding to the strongest warming rate (see Fig. 1b). Also for 2C30 and 2C25 the strongest change rates of about 0.2 mm/d/century occur at about the same time as the strongest warming rates (around 2030), while for 2C20 the strongest change in precipitation occurs later than for the near-surface temperature. The latter is caused by a very small increase in daily precipitation over the land areas in the period 2015-2030 presumably due to variability on decadal time scales, while such a variation of the change rate does not occur over the oceans. A similar variation occurs also for 2C30A with

change rates of 0.05 mm/d/century between 2015 and 2030. In this case the daily precipitation over the land areas actually decreases for several years.

## Precipitation

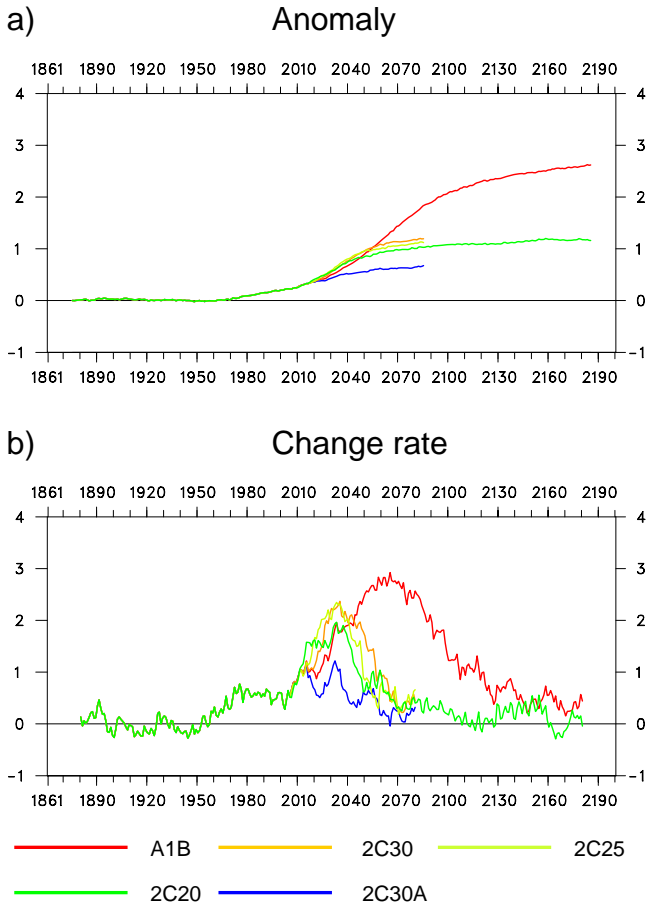


**Figure 2:** As Fig. 1, but for daily precipitation with a value of 2.91 mm/d for the reference period. Units are [1/10 mm/d] (a) and [1/10 mm/d/century] (b).

### 3.3 Sea-ice conditions

For the sea-ice cover and sea-ice volume in the Arctic and the Antarctic region, semi-annual means are considered, distinguishing between the periods January through June (“Jan-Jun”) and July through December (“Jul-Dec”). Only grid boxes with at least 15% of the area covered by sea-ice in a particular month are included.

In the Arctic region, A1B shows a considerable reduction of the sea-ice cover with respect to pre-industrial times by about 4,000 km<sup>2</sup> in Jan-Jun (Fig. 3a) and about 6,000 km<sup>2</sup> in Jul-Dec by the end of the 21<sup>st</sup> century (Fig. 3b). By the end of the 22<sup>nd</sup> century the reduction has reached 5,000 km<sup>2</sup> in Jan-Jun and about 7,500 km<sup>2</sup> in Jul-Dec, corresponding to a reduction of 40% in the first half but 90% in the second half of the year, respectively. Apparently, the sea-ice cover is more sensitive to global warming in the part of the year with the smallest sea-ice extent (Jul-Dec) than in the period with the largest extent (Jan-Jun). In 2C20 the reduction of the Arctic sea-ice cover is markedly weaker, about 2,200 km<sup>2</sup> (17%) in Jan-Jun and 3,000 km<sup>2</sup> (36%) in Jul-Dec, again with the strongest reduction in the period with the smallest sea-ice extent. For 2C20 the sea-ice cover reaches its equilibrium well before the end of the 21<sup>st</sup> century, while in A1B the sea-ice cover continues to steadily decrease by the end of the 22<sup>nd</sup> century. Also the effect of the higher aerosol emissions on

the sea-ice cover is stronger in Jul-Dec than in Jan-Jun, with a difference between 2C30 and 2C30A of about 1,200 km<sup>2</sup> in Jul-Dec and of about 500 km<sup>2</sup> in Jan-Jun.

### Sea-ice conditions—Northern Hemisphere

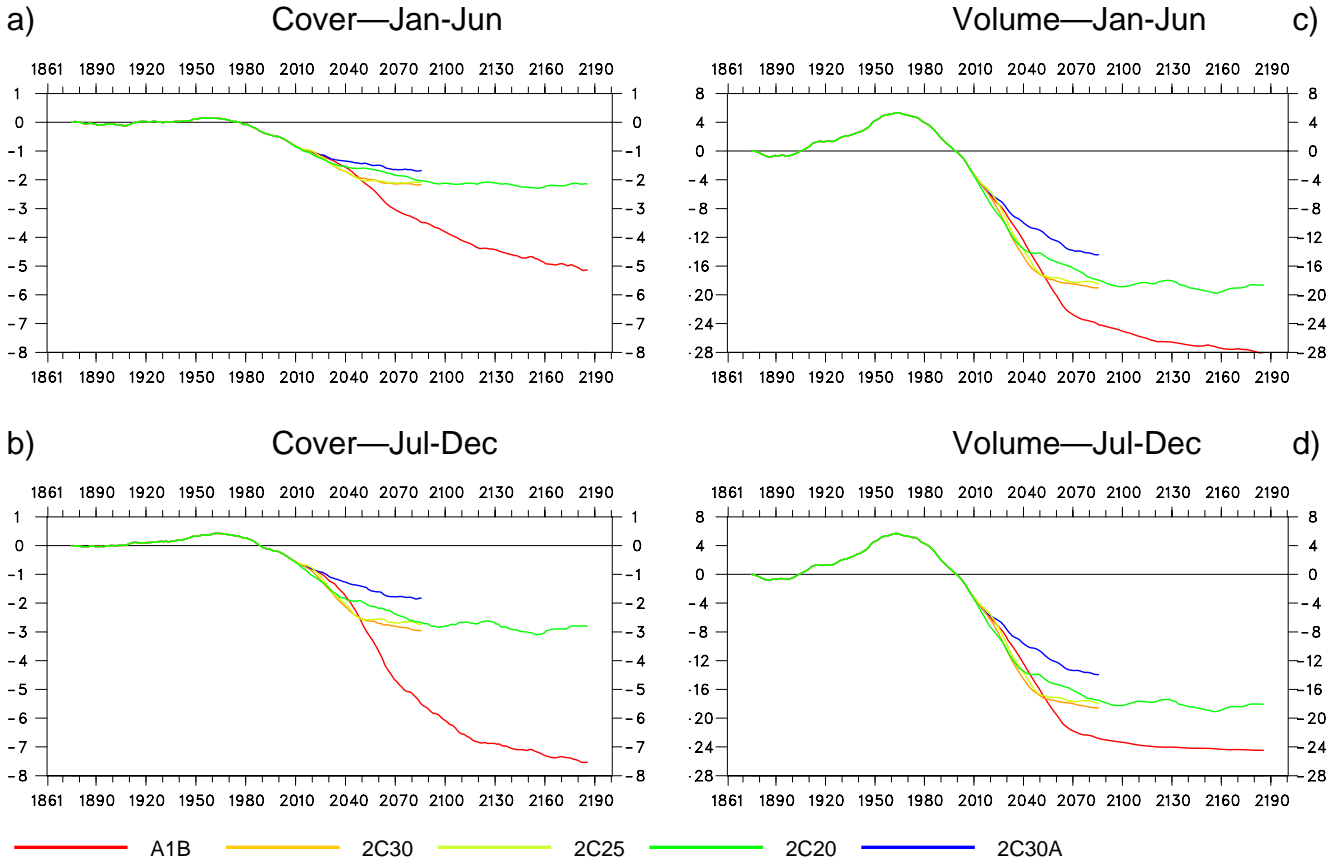


**Figure 3:** Changes in the 30-year averages of semi-annual mean sea-ice cover (a, b) and sea-ice volume in the Arctic region with respect to the period 1861-1890 for January-June (“Jan-Jun”; left column) and July-December (“Jul-Dec”; right column) and the different experiments. The values for the reference period are 12,730 (Jan-Jun) and 8,300 km<sup>2</sup> (Jul-Dec) for the sea-ice cover as well as 35,000 (Jan-Jun) and 24,900 km<sup>3</sup> (Jul-Dec) for the sea-ice volume. Units are [1000 km<sup>2</sup>] (a, b) and [1000 km<sup>3</sup>] (c, d).

For the sea-ice volume (Figs. 3c, d) the changes with respect to pre-industrial times by the end of the 22<sup>nd</sup> century are considerably stronger than for the sea-ice cover, with a reduction of 80% in Jan-Jun and 96% in Jul-Dec in A1B, leaving only about 900 km<sup>3</sup> of sea-ice in the second half of the year. In 2C20 the sea-ice cover is not as strongly reduced, i.e., 54% in Jan-Jun and 72% in Jul-Dec, but also in this simulation the reduction of the sea-ice volume is markedly stronger than for the sea-ice cover. Apparently, not only the sea-ice extent is reduced due to global warming but also the thickness, particularly in the first half of the year, when the sea-ice develops. It is interesting to note that also in A1B the sea-ice volume in Jul-Dec reaches its equilibrium around 2100. In contrast to the sea-ice cover, the effects of the higher aerosol emissions on the sea-ice volume have the same magnitude (about 6,000 km<sup>3</sup> larger sea-ice volume in 2C30A) in the two halves of the year. In the first half of the year the cooling effect of the aerosols apparently has a stronger impact on the accumulation of sea-ice once it has developed than on the development.

Also in the Antarctic region, A1B shows a strong reduction of the sea-ice cover by the end of the 22<sup>nd</sup> century, by about 3,600 km<sup>2</sup> in Jan-Jun and about 7,800 km<sup>2</sup> in Jul-Dec (Figs. 4a, b), corre-

sponding to 76% (Jan-Jun) and 64% (Jul-Dec) of the values for pre-industrial times. Similarly, the Antarctic sea-ice volume is reduced (Figs. 4c, d) by 85% in Jan-Jun and 71% in Jul-Dec, that is to a somewhat larger extent than the sea-ice cover. In 2C20 the reductions in both the sea-ice cover and the sea-ice volume are about half as large as in A1B, leaving a sea-ice cover of about 2,800 km<sup>2</sup> in Jan-Jun and of about 8,900 km<sup>2</sup> in Jul-Dec by the end of the 22<sup>nd</sup> century. In contrast to the Arctic region, the higher aerosol emissions in 2C30A do not affect the simulated changes of the sea-ice conditions in the Antarctic region.

## Sea-ice conditions—Southern Hemisphere

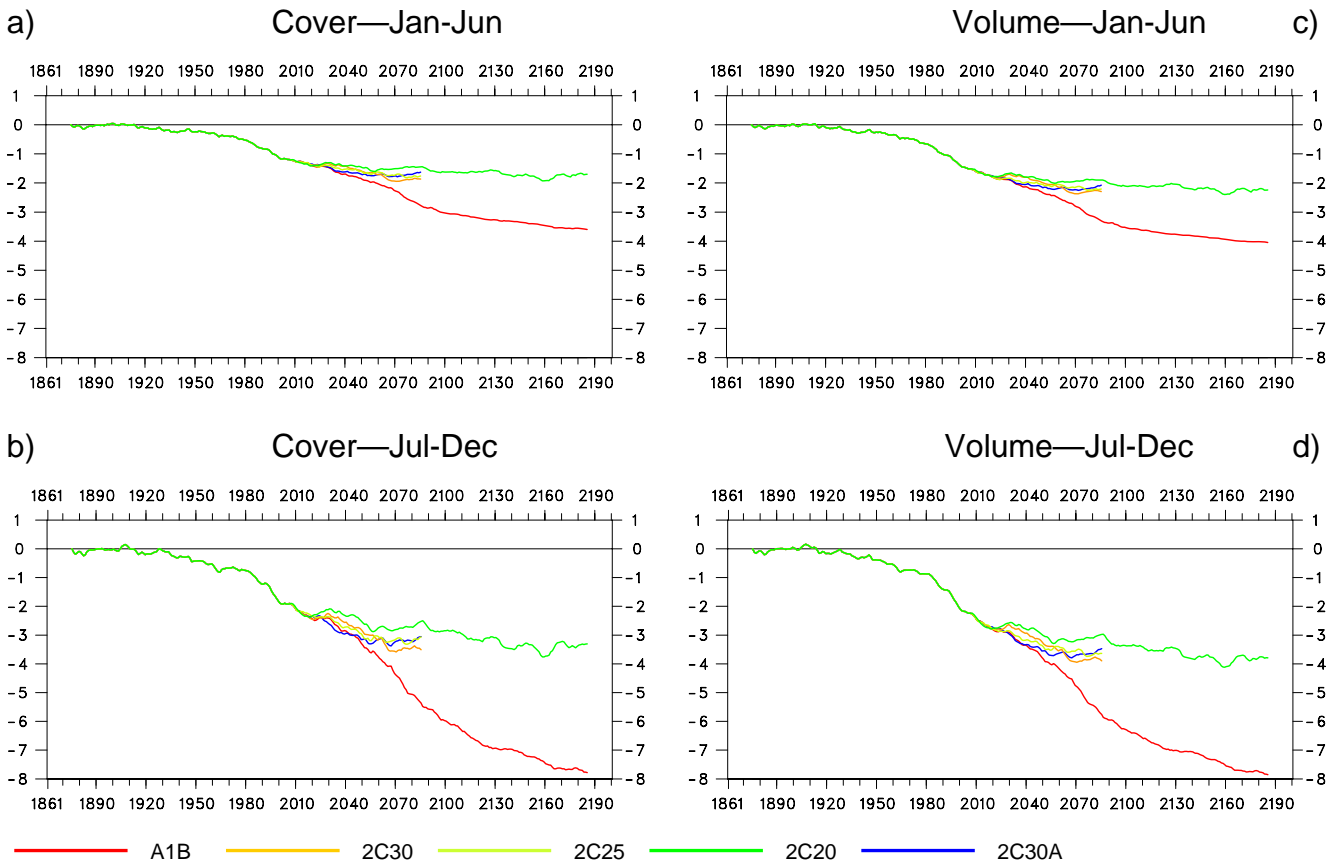


**Figure 4:** As Fig. 3, but for the Antarctic region with values of 4,640 (Jan-Jun) and 12,100 km<sup>2</sup> (Jul-Dec) for the sea-ice cover as well as 4,730 (Jan-Jun) and 11,010 km<sup>3</sup> (Jul-Dec) for the sea-ice volume for the reference period.

## 4. Zonal mean changes

### 4.1 Near-surface variables

In this section, the changes in the zonal means of the annual mean values between the periods 2071-2100 and 1961-1990 are presented for some near-surface variables, considering four of the experiments (A1B, 2C20, 2C30, and 2C3A).

The future warming due to enhanced greenhouse gas concentrations is generally not equally distributed over the globe but more pronounced at the high latitudes, in particular in the Northern Hemisphere (e.g., Cubasch et al. 2001). This is also the case in the experiments shown here, with the warming in the high northern latitudes exceeding 8 °C for A1B and reaching about 4 °C in the other experiments (Fig. 5a). At the other latitudes, 2C20 shows a warming at about 2 °C, except for the

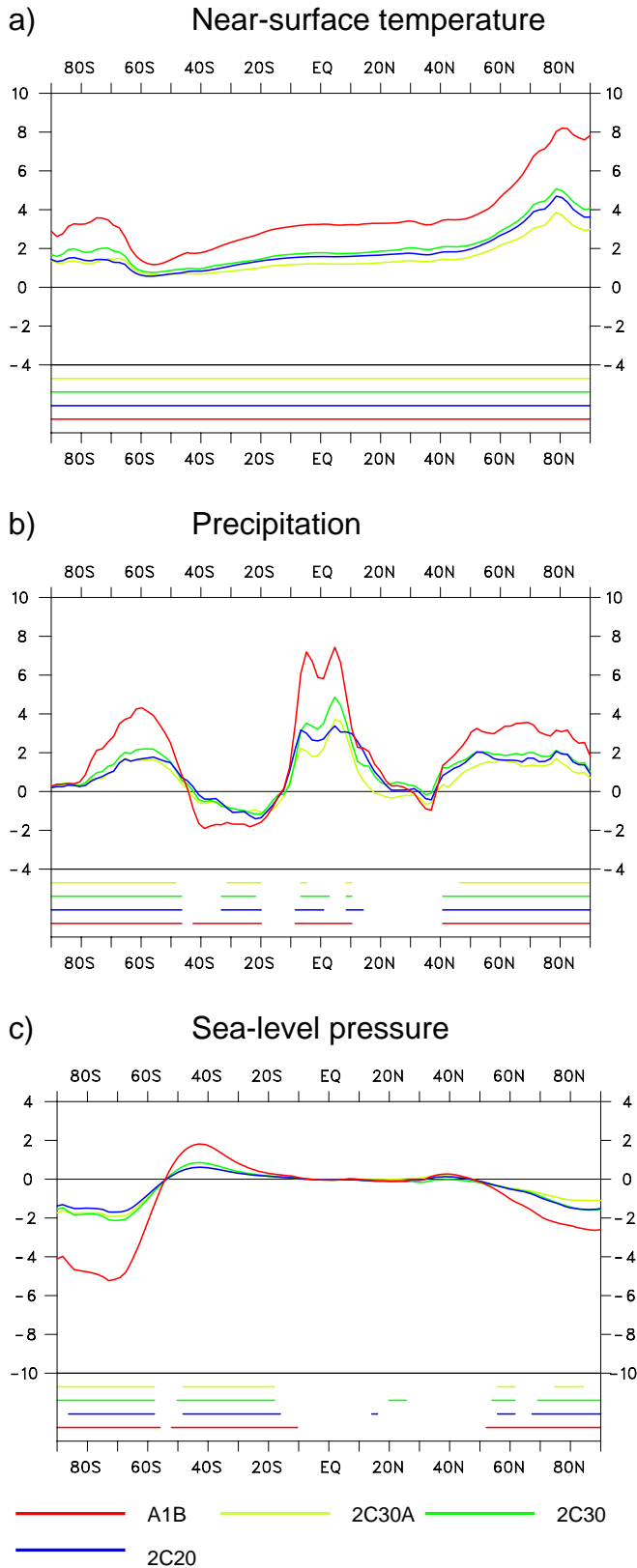


**Figure 5:** Changes in the annual mean zonal means between the periods 1961-1990 and 2071-2100 for the annual means of a) the annual mean near-surface temperature, b) daily precipitation, and c) sea-level pressure for A1B, 2C30, 2C30A and 2C20. The significance of these changes at the 99.0 %-level (a, b) and the 97.5% level (c) is indicated by the horizontal lines. Units are [°C] (a), [1/10 mm/d] (b), and [hPa] (c).

mid-latitudes in the Southern Hemisphere with a warming of about 1 °C. By this, the warming in 2C20 is generally about half as strong as for A1B. The higher aerosol emissions in 2C30A lead to a somewhat weaker warming than for 2C30, i.e., 1 °C in the high northern latitudes and 0.5 °C elsewhere.

As a consequence of the warming, all experiments give a marked increase in daily precipitation in the tropics as well as in the mid- and high latitudes of both hemispheres (Fig. 5b). In the Southern Hemisphere, precipitation is reduced in the entire subtropics, while in the Northern Hemisphere only 2C30A shows a general decrease in the subtropics. All other experiments give a slight decrease at about 35° N, but none of the changes in the Northern Hemisphere subtropics are statistically significant. In A1B the changes are about twice as strong as in the other experiments, with increases of 0.7 mm/d in the tropics and about 0.4 mm/d in the mid- and high latitudes. 2C20 shows increases of 0.3 mm/d in the tropics and of 0.2 mm/d in the extratropics and a decrease of 0.1 mm/d in the Southern Hemisphere subtropics. The higher aerosol emissions in 2C30A lead to weaker increases of daily precipitation in all regions except for the Southern Hemisphere subtropics and to a decrease in the Northern Hemisphere subtropics.

Further, all experiments show a decrease of the sea-level pressure in part of the mid- and at the high latitudes of both hemispheres, i.e., north and south of 50° N and 55° S, respectively (Fig. 5c). In A1B the decrease in the Antarctic region is about twice as strong as in the Arctic region, but for 2C20 the corresponding changes have a similar magnitude in both hemispheres. In the Southern Hemisphere extratropics the sea-level pressure is significantly increased, particularly in A1B, while in the Northern Hemisphere such an increase is hardly visible. As for the impact of the high aerosol emissions, the only marked difference between 2C30A and 2C30 is the somewhat weaker decrease of the sea-level pressure in the Arctic region. The future changes in the sea-level pressure indicate a marked amplification of the pressure gradient between the mid- and the high latitudes, particularly in the Southern Hemisphere.

## 4.2 Latitude-height cross sections

In this section, latitude-height cross sections for the annual mean temperature and zonal wind component are presented, i.e., the changes between the periods 2071-2100 and 1961-1990 for A1B and 2C20 as well as the differences between A1B and 2C20 and between 2C30 and 2C30A, respectively, for the period 2071-2100.

For the future, both A1B and 2C20 show a warming in the troposphere and a cooling in the stratosphere, particularly at the high latitudes (Figs. 6a, b). The strongest warming with more than 6 °C in A1B and more than 3 °C in 2C20, respectively, occurs in two areas, the upper troposphere in the tropical region and the lower troposphere in the Arctic region. The weakest warming with less than 2 °C in A1B and less than 1 °C for 2C20 occurs over the oceans in the Southern Hemisphere in the lower and mid-troposphere. By this, the future changes simulated in these two experiments correspond very well to the respective changes presented in the 3<sup>rd</sup> IPCC-report (Cubasch et al. 2001). The aforementioned changes in the temperature distribution lead to a strengthening of the meridional temperature gradient in the upper troposphere and in the stratosphere in both hemispheres. In the Northern Hemisphere, the meridional temperature gradient is markedly reduced in the lower troposphere, while in the Southern Hemisphere the meridional temperature gradient is enhanced throughout the troposphere.

The differences between A1B and 2C20 for the period 2071-2100 have a very similar structure as the future changes simulated in 2C20 but are somewhat stronger, except for the lower troposphere in the Arctic region with a maximum warming of 3 °C (Fig. 6c). 2C30, on the other hand, is warmer than 2C30A almost everywhere, including the stratosphere at the high latitudes in both hemispheres

(Fig. 6d). In the lower and mid-troposphere of the Northern Hemisphere, the differences are about twice as large as in the Southern Hemisphere, indicating that the higher aerosol emissions lead to a more pronounced cooling in the Northern than in the Southern Hemisphere. This is due to the relatively large aerosol concentrations in the Northern Hemisphere extratropics. The stratospheric warming at the high latitudes, on the other hand, is caused by the higher ozone concentrations in 2C30, about 25% in the mid-stratosphere.

## Temperature

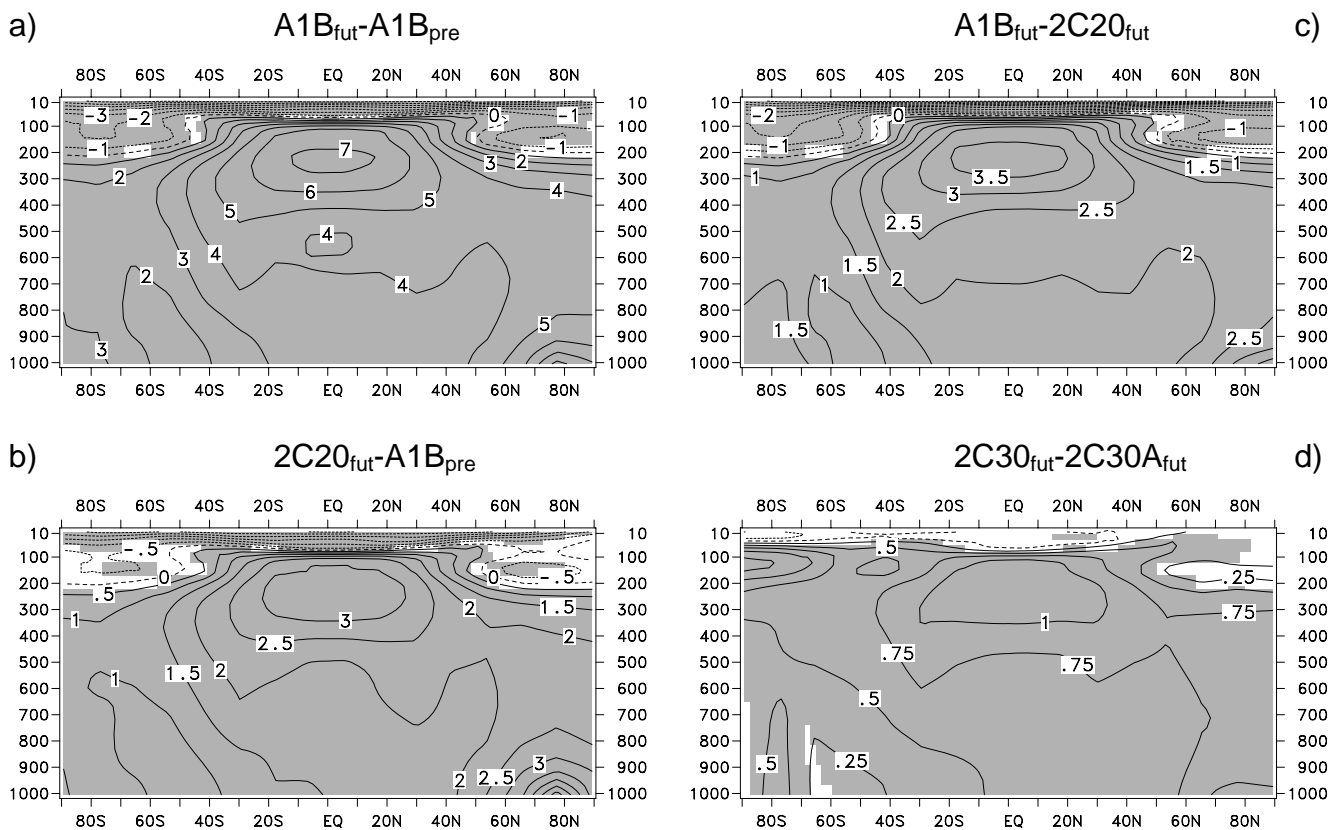


**Figure 6:** Changes in the annual mean zonal means of temperature between the periods 1961-1990 and 2071-2100 for a) A1B and b) 2C20 as well as the differences c) between A1B and 2C20 and d) between 2C30 and 2C30A. The significance of these changes at the 99.0 % level (a-c) and the 97.5 % level (d) is indicated by the shading. Units are [ $^{\circ}\text{C}$ ], the contour interval is  $1^{\circ}\text{C}$  (a),  $0.5^{\circ}\text{C}$  (b, c), and  $0.25^{\circ}\text{C}$  (d).

As a consequence of the future strengthening of the meridional temperature gradient, both A1B and 2C20 show marked increases in the westerly winds in the stratosphere between 20 and 60° northern and southern latitude, respectively (Figs. 7a, b). This leads to an intensification of the subtropical jet streams in both hemispheres, with the zone of relatively strong westerly winds extending further into the stratosphere. Furthermore, the westerly winds intensify throughout the troposphere in the Southern Hemisphere extratropics, so that the zone of the relatively strong westerly winds is extended further southward. In the tropics, on the other hand, the two experiments show a slight weakening of the easterly winds throughout the troposphere.

Consistent with the larger magnitude of the temperature differences between A1B and 2C20 for the period 2071-2100 compared to the future changes simulated in 2C20, also the corresponding differences in the zonal wind component are relatively large (Fig. 7c). This is particularly the case in the Southern Hemisphere, where the differences between A1B and 2C20 are about twice as large as the

change simulated in 2C20. The differences in the anthropogenic aerosol emissions have only a minor impact on the zonal wind component, with weaker westerly winds in the stratosphere roughly between 50° S and 60° N in 2C30A (Fig. 7d), consistent with the reduced meridional temperature gradient in the stratosphere in this simulation (see Fig 6d). Furthermore, the easterly winds are enhanced in the mid-troposphere of the tropical region.

## Zonal wind component

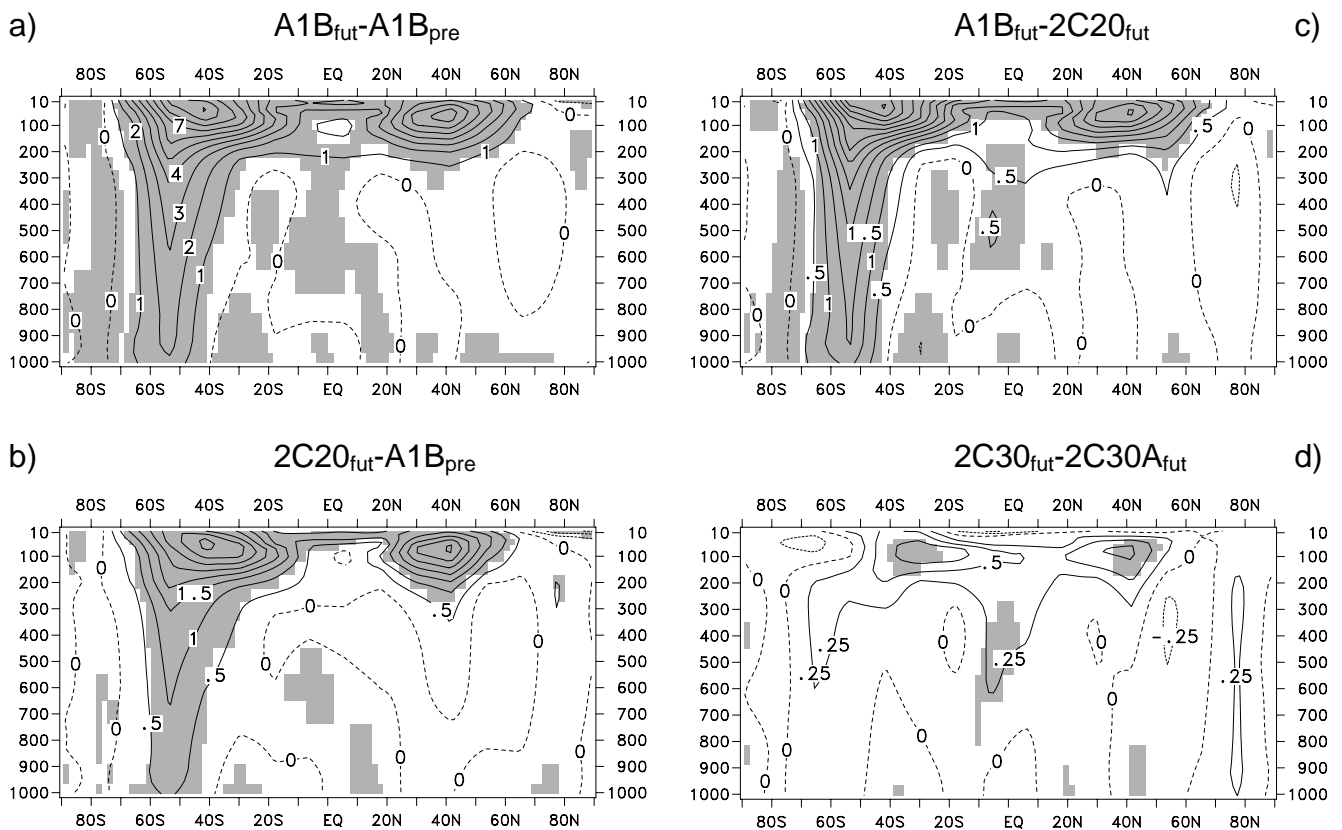


**Figure 7:** As Fig. 6, but for the zonal wind component. The significance levels are at 97.5 % (a-c) and at 95 % (d). Units are [m/s], the contour interval is 1 m/s (a), 0.5 m/s (b, c), and 0.25 m/s (d).

## 5. Local changes

### 5.1 Sea-ice conditions

Consistent with the previous discussion of the sea-ice conditions, semi-annual means for the periods January through June (“Jan-Jun”) and July through December (“Jul-Dec”) are considered for the local changes in the sea-ice conditions. These are the 6-month periods with the largest and smallest sea-ice extent in the polar regions. Again, only grid-boxes with at least 15% of the area covered by sea-ice are included.

In Jan-Jun, all simulations show a reduction in the sea-ice cover and in the sea-ice thickness due to the increased greenhouse gas emissions in both hemispheres (Fig. 8). The sea-ice has particularly retreated in the Barents Sea, the Sea of Okhotsk and the Bering Sea in the Arctic region and in the Ross Sea and the Weddell Sea in the Antarctic region. The sea-ice thickness, on the other hand, is most markedly reduced in the East Siberian Sea and the Beaufort Sea in the Arctic and in the Weddell Sea in the Antarctic region. A1B, the experiment with the strongest future warming, shows the most pronounced changes in the sea-ice conditions, with the Hudson Bay and a small part of the

## Sea-ice conditions—Jan-Jun

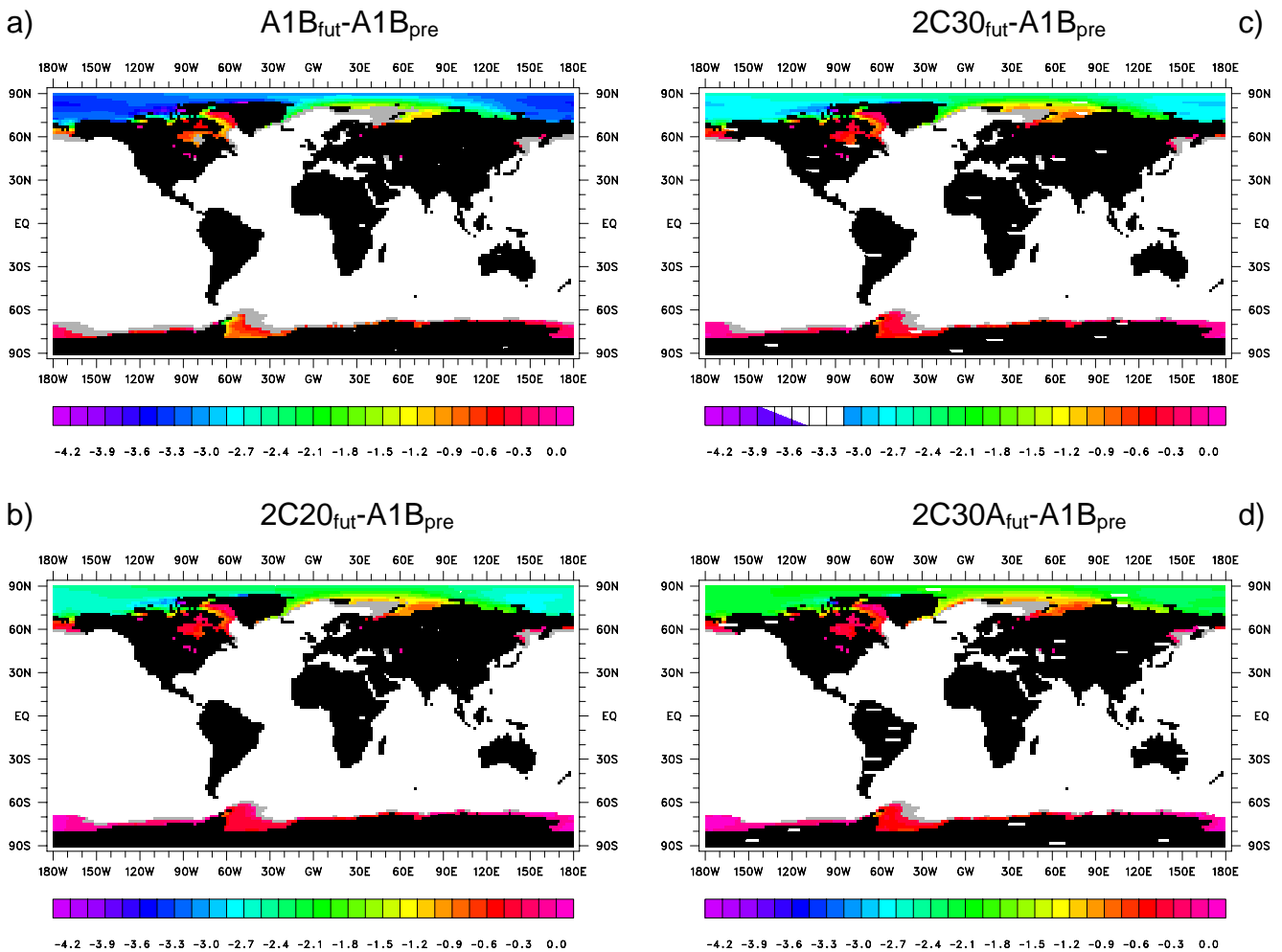


**Figure 8:** Changes in the 30-year averages of semi-annual (January-June) mean sea-ice cover and sea-ice thickness between the periods 1961-1990 and 2071-2100 for a) A1B, b) 2C20, c) 2C30 and d) 2C30A. Marked in grey are those areas that are covered with sea-ice only during 1961-1990 and in the other colours those areas that are covered with sea-ice during both periods. Units are [m] for the sea-ice thickness, the contour interval is 0.15 m.

Kara Sea without any sea-ice in Jan-Jun and particularly strong changes in the Arctic region, namely a marked retreat of the sea-ice extent in the Ross and the Weddell Sea and a marked thinning of the sea-ice in the Weddell Sea (Fig. 8a). As a consequence of the weaker future warming, the changes in the sea-ice conditions are somewhat weaker in the three other experiments. In the Arctic region, the magnitude of the changes in the sea-ice conditions follows the changes in the global mean temperatures with the largest changes in 2C30 (Fig. 8c) and the weakest changes in 2C30A (Fig. 8d). In 2C20, the Kara Sea and much of the Sea of Okhotsk are no longer covered with sea-ice in Jan-Jun (Fig. 8b). In the Antarctic region, on the other hand, the changes in the sea-ice conditions are weaker in 2C20 (Fig. 8b) than in 2C30A (Fig. 8d), particularly in the Weddell Sea, despite the significantly stronger global warming in 2C20. This indicates that in the high southern latitudes the effect of the higher greenhouse gas concentrations in 2C30A compensates for the impact of the higher aerosol emissions.

Also in Jul-Dec, all simulations show a future reduction in the sea-ice extent and the sea-ice thick-

ness in both hemispheres (Fig. 9). The sea-ice has particularly retreated in the Baffin Bay and the Kara Sea in the Arctic region and in the Weddell Sea in the Antarctic region. The sea-ice thickness is markedly reduced in the East Siberian Sea and the Beaufort Sea and in the area north of the Canadian Archipelago. In the Antarctic region, on the other hand, all experiments show an almost uniform thinning of the sea-ice by about 30 cm. In A1B, the simulation with the strongest changes in the sea-ice conditions, the Fox Basin and the Baffin Bay are without sea-ice in Jul-Dec, and there is no longer sea-ice in the Chukchi Sea and the southern part of the Beaufort Sea as well as in parts of the Laptev Sea (Fig. 9a). Also, A1B is the only simulation with the sea-ice extent retreating far to the north of Svalbard. In the Antarctic region, A1B shows also a marked reduction in the sea-ice extent in the Ross Sea and in the Amundsen Sea. Similar to Jan-Jun, the magnitude of the changes in the sea-ice conditions in the Arctic region follows the magnitude of the future changes in the global mean temperature, while in the Antarctic region 2C20 shows the weakest changes in the sea-ice conditions. In 2C20, the Chukchi Sea and the Beaufort Sea and the western part of the Baffin Bay are still covered with sea-ice (Fig. 9b). This is also the case for the Laptev Sea and to a large extent for the area north of Svalbard.

### Sea-ice conditions—Jul-Dec

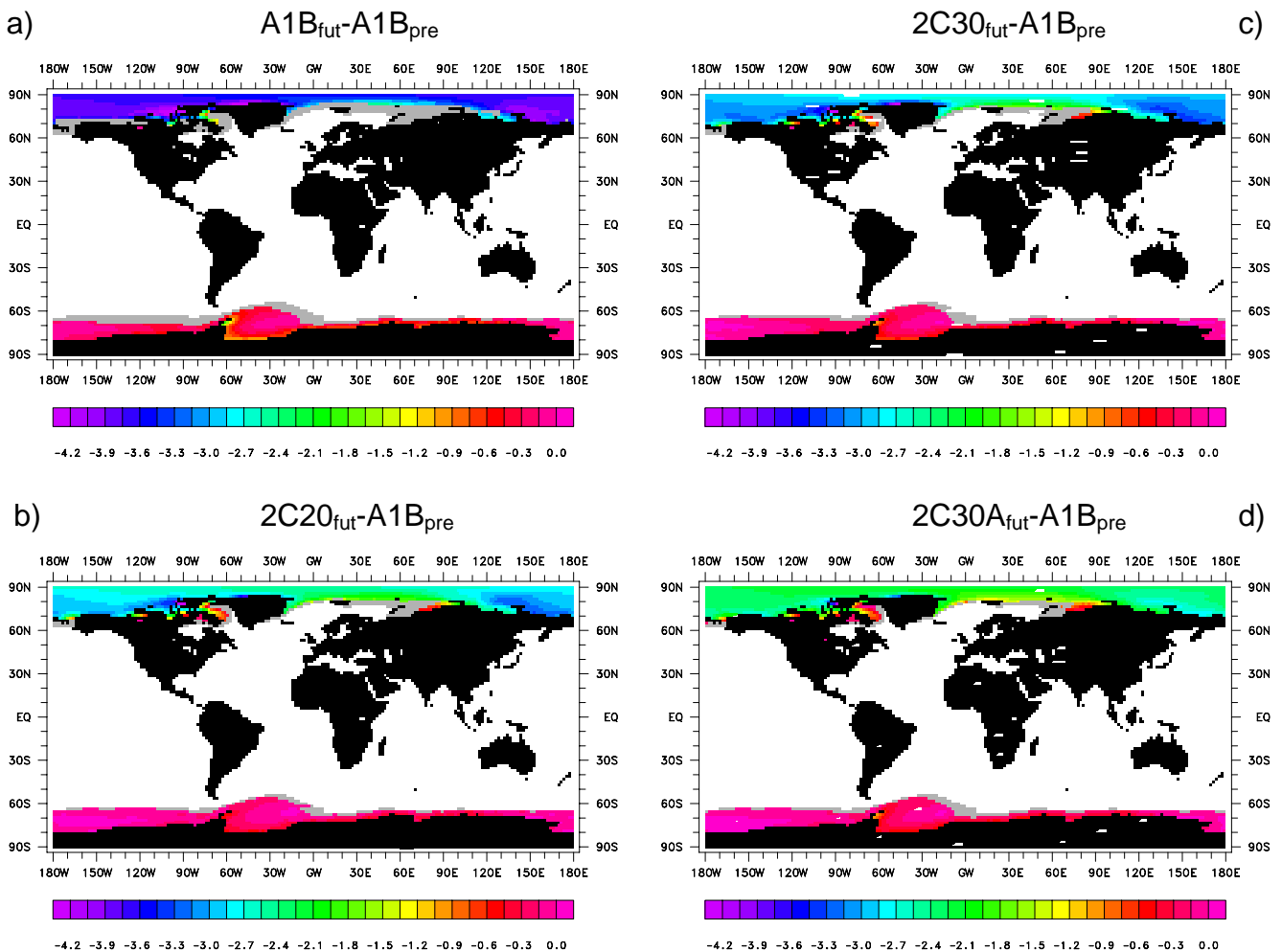


**Figure 9:** As Fig. 8, but for July-December.

However, the local changes in the sea-ice conditions due an increase in the greenhouse gas concentrations can vary considerably from model to model and, hence, can be uncertain to some extent. In Cubasch et al. (2001), for instance, three out of the four models presented show a strong reduction

of the sea-ice thickness in different parts of the area north of Greenland and Canada, while one model shows a strong reduction in the sea-ice thickness in the area north of the Barents Sea and the Kara Sea but a thickening of the sea-ice in the area north of Alaska and western Canada. As for the Antarctic region, all these models show a marked reduction in the sea-ice thickness in the Weddell Sea and, again, three out of four a strong reduction in the Ross Sea as well.

## 5.2 Near-surface temperature

### Near-surface temperature

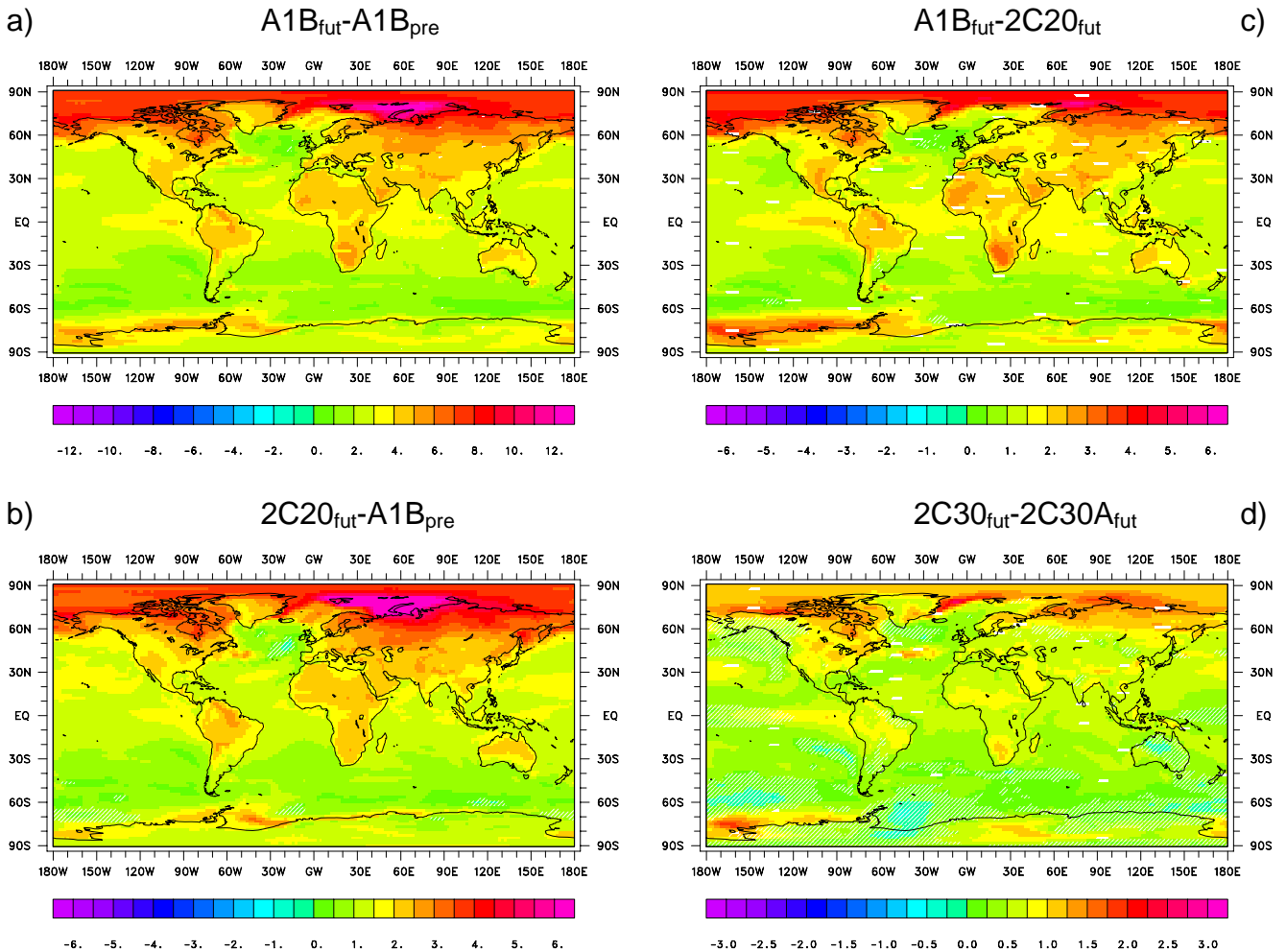


**Figure 10:** Changes in the annual mean near-surface temperature between the periods 1961-1990 and 2071-2100 for a) A1B and b) 2C20 as well as the differences c) between A1B and 2C20 and d) between 2C30 and 2C30A. The areas where these changes are not significant at the 99.0 % level (a-c) and the 97.5 % level (d) are marked by the white stippling. Units are [°C], the contour interval is 1 °C (a), 0.5 °C (b, c), and 0.25 °C (d).

Consistent with the future changes in the zonal means of the annual mean near-surface temperature (see Fig. 5a), A1B shows a pronounced warming due to the increased greenhouse gas concentrations in the Arctic region, exceeding 6 °C over most of the area but reaching more than 12 °C over the Barents Sea and the Kara Sea (Fig. 10a). This strong warming is related to the positive ice-albedo-feedback in the Arctic region as a consequence of the retreating sea-ice (see Figs. 8a, 9a). Particularly in the Barents Sea and the Kara Sea, the simulations show a strong retreat of the sea-ice, most pronounced in the second half of the year. The ice-albedo-feedback is also the reason for the

relatively strong warming over the Ross Sea and the Weddell Sea in the Antarctic region. Except for the high latitudes, the warming is stronger over the land areas, generally exceeding 4 °C, than the adjacent ocean basins due to higher heat capacity of the oceans. In northern Canada and in northern Russia the warming is further enhanced by the positive snow-albedo-feedback as a consequence of the shortened period with snow at the ground. As for the oceans, A1B shows a pronounced warming in the eastern tropical Pacific Ocean, similar to the sea-surface temperature anomaly during an El Niño event, and a very small warming in the Atlantic Ocean, roughly between the southern tip of Greenland and the British Isles, as well as in the Southern Ocean. The latter is related to the strong vertical mixing of the water masses in these ocean basins. This distribution of the future changes in the annual mean near-surface temperatures has many features in common with corresponding simulations by other climate models (e.g., Cubasch et al. 2001). However, only part of these models simulate the El Niño-like warming pattern in the eastern tropical Pacific Ocean and most models give a stronger warming in the Atlantic Ocean to the west of the British Isles.

2C20 (Fig. 10b) shows a similar pattern of the future change in the near-surface temperature but the magnitude is about half as strong as for A1B. However, the warming over the Barents Sea and the Kara Sea is relatively strong, exceeding 8 °C, which is markedly more than half of the 12 °C for A1B in this region. 2C20 does not show such a pronounced El Niño-like warming pattern in the eastern tropical Pacific Ocean as A1B. This is particularly evident in the distribution of the differences between A1B and 2C20 (Fig. 10c) with a tongue of positive temperature differences centred on the equator in the eastern Pacific Ocean. This is part of a general pattern with a less pronounced warming also in the tropical Atlantic Ocean and Indian Ocean as well as in subtropical Africa, Saudi Arabia and parts of India. In contrast to A1B, 2C20 actually shows a slight (non-significant, though) cooling in the Atlantic west of the British Isles (Fig. 10b), indicating that only relatively strong greenhouse gas emissions lead to a future warming in this part of the Atlantic Ocean.

The effect of the higher aerosol emissions in 2C30A on the near-surface temperatures has a similar signature (with the opposite sign) as the warming due to increased greenhouse gas concentrations. The distribution of the differences between 2C30 and 2C3A (Fig. 10d) shows a relative strong warming in the high northern latitudes, mainly at the southern edge of the sea-ice area, and an El Niño-like warming pattern in the eastern tropical Pacific Ocean. In the Southern Oceans the higher aerosol emissions do generally not have a significant effect on the near-surface temperatures. Systematic local effects in the vicinity of the regions with a strong production of sulphate aerosols, i.e., in the industrialized areas in the Northern Hemisphere midlatitudes and in parts of the subtropics, are hard to find, presumably since they are overruled by the natural climate variability. The distribution shows, however, a marked warming over eastern North America, eastern China and South Africa in 2C30 due to the lower aerosol emissions, but not in Europe and Russia. The distribution of the differences shown here is very similar to the one in Brasseur and Roeckner (2005), except that they found a larger effect of higher aerosol emissions in Europe and Russia.

### 5.3 Precipitation

As for daily precipitation, A1B shows an increase in the tropical region and in the mid- and high latitudes and a reduction in the subtropical regions (Fig. 11a), again consistent with the future changes in the zonal means of daily precipitation (see Fig. 5b). The changes in the tropical and subtropical regions are caused by enhanced convergence of the large-scale flow and intensified upward motions with more precipitation in the tropics causing, in turn, intensified downward motions with less precipitation in the subtropics. The increases in the mid- and high latitudes, on the other hand, are due to an increase in the precipitation intensity within low-pressure systems as a consequence of the generally enhanced atmospheric moisture content in the future. The most pronounced increase occurs over the tropical Pacific Ocean in association with the El Niño-like

warming pattern in this ocean basin (see Fig. 10a). This increase in precipitation is accompanied by decreases over Indonesia, the subtropical parts of the Pacific Ocean and Central America. Such future changes in daily precipitation are a common feature in many climate models (e.g., Cubasch et al. 2001).

## Precipitation

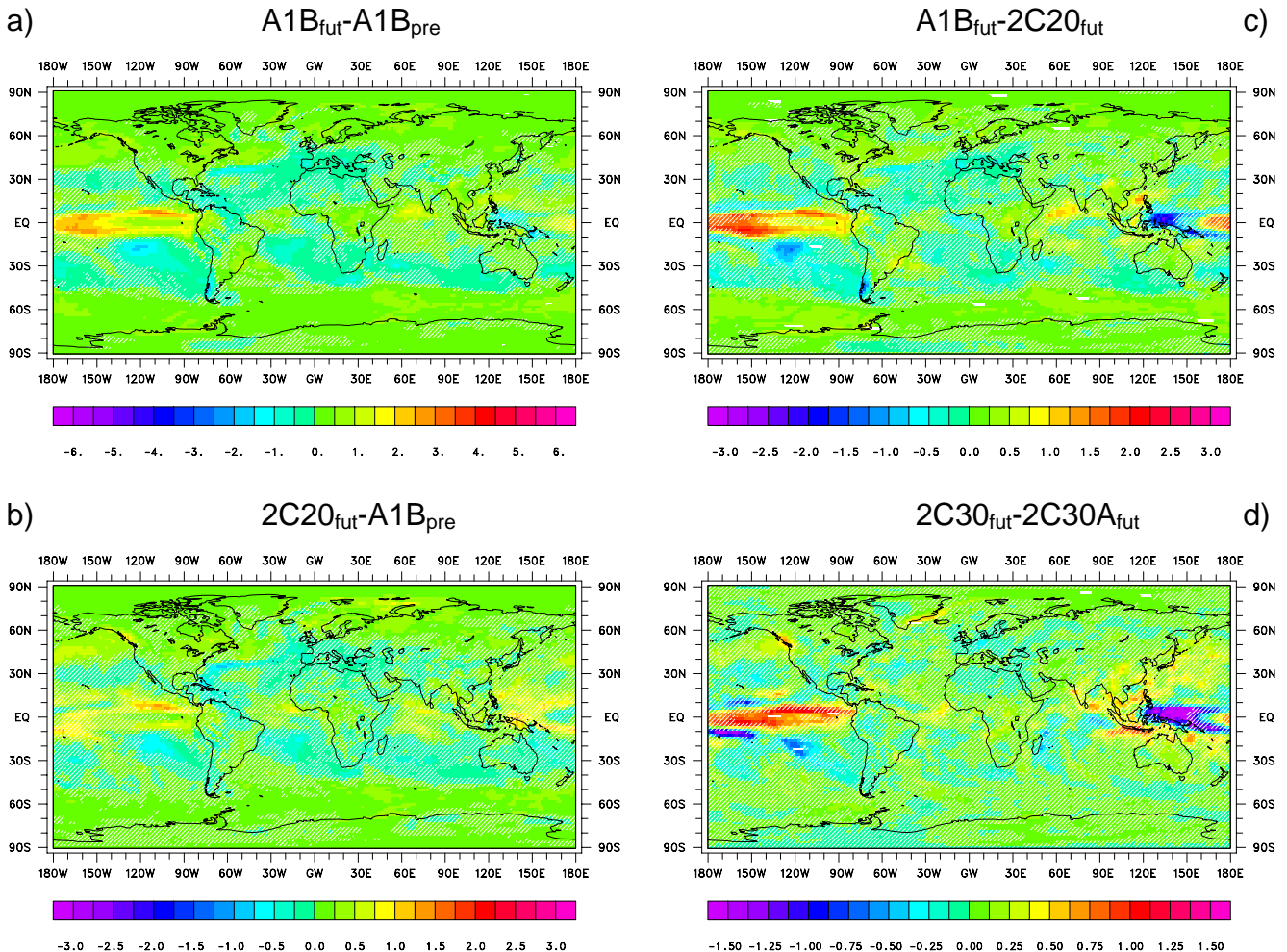


**Figure 11:** As Fig. 10, but for daily precipitation. The significance levels are at 97.5 % (a-c) and at 95 % (d). Units are [mm/d], the contour interval is 0.5 mm/d (a), 0.25 mm/d (b, c), and 0.125 mm/d (d).

In 2C20 (Fig. 11b) the future changes in daily precipitation have a similar structure as in A1B but the magnitude of the changes is generally about half as strong as in A1B. The increase over the tropical Pacific Ocean, however, is less pronounced in 2C20 due to the less pronounced El Niño-like warming pattern in this experiment (see Fig. 10b). In contrast to A1B, precipitation is actually enhanced over Indonesia. The latter is also one of the most pronounced features in the distribution of the differences between A1B and 2C20 (Fig. 11c). This figure also illustrates that the substantial reduction of daily precipitation in the Mediterranean region is stronger in A1B than in 2C20.

Similar to the near-surface temperature, the effect of the higher aerosol emissions on daily precipitation (Fig. 11d) also has a similar structure (with the opposite sign) as the changes due to the increased greenhouse gas concentrations. The most pronounced difference between 2C30 and

2C30A is enhanced precipitation over the tropical Pacific Ocean and the associated reduction over Indonesia in 2C30, again associated with the marked El Niño-like warming pattern in 2C30 (see Fig. 10d). Apparently, the most important effect of the higher aerosol emissions in 2C30A is to weaken the most robust climatic changes as a response to the weaker global warming. The local effects of the higher aerosol emissions, on the other hand, are less important, particularly for such a strongly changing meteorological variable as precipitation.

## 5.4 Sea-level pressure

### Sea-level pressure

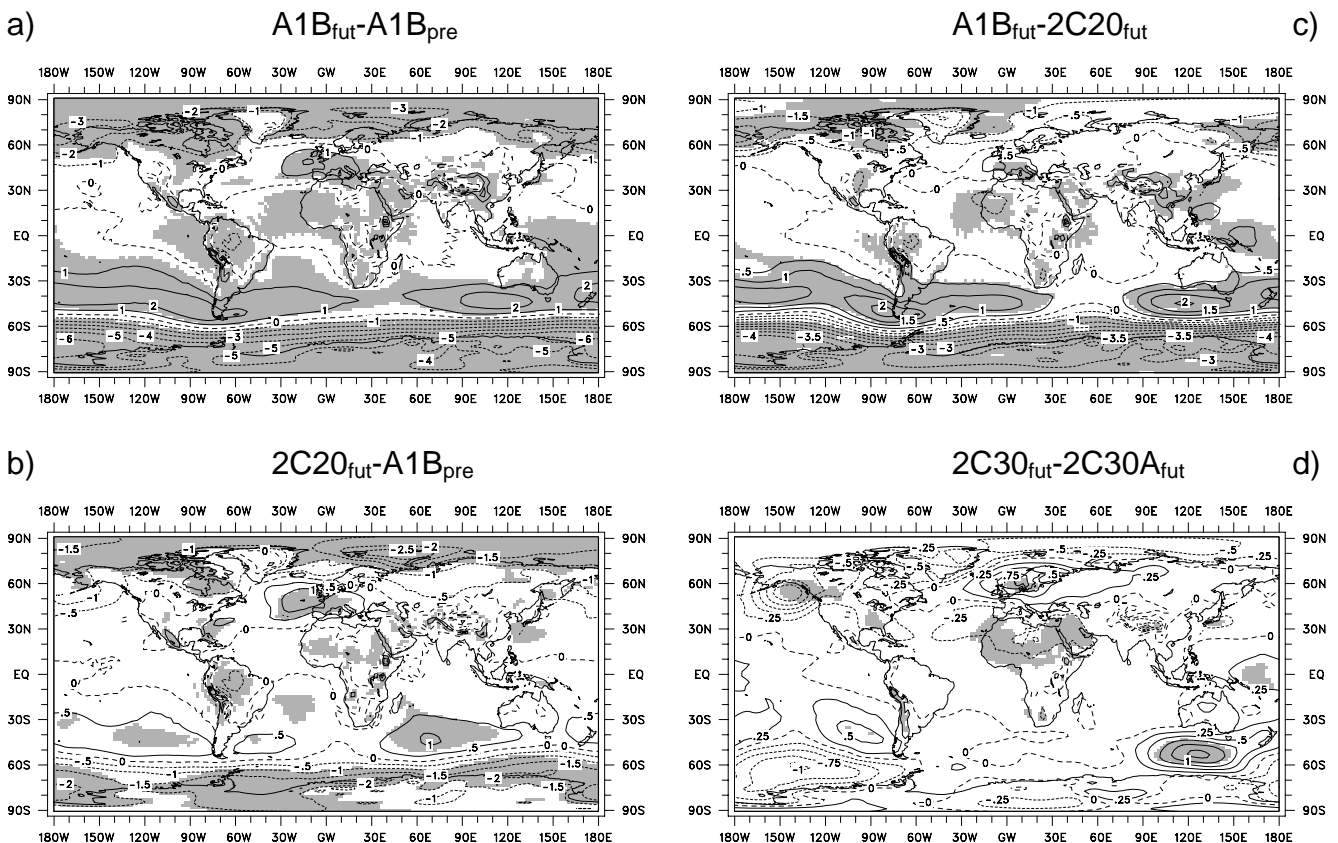


**Figure 12:** Changes in the annual mean sea-level pressure between the periods 1961-1990 and 2071-2100 for a) A1B and b) 2C20 as well as the differences c) between A1B and 2C20 and d) between 2C30 and 2C30A. The significance of these changes at the 99.0 % level (a-c) and the 97.5 % level (d) is indicated by the shading. Units are [hPa], the contour interval is 1 hPa (a), 0.5 hPa (b, c), and 0.25 hPa (d).

For the future, A1B shows a pronounced reduction of the sea-level pressure in the high latitudes of both hemispheres and an increase in the mid-latitudes (Fig. 12a). In the tropics, the atmospheric pressure is reduced in one half of the globe, reaching from the eastern Pacific Ocean over South America, the Atlantic Ocean and Africa into the western Indian Ocean, and enhanced in the other half. In the Southern Hemisphere mid-latitudes, these changes indicate a southward shift of the predominant ridge-trough system, with ridges located west of South America over the South Pacific Ocean, between South America and Africa over the South Atlantic Ocean and between Africa and Australia over the South Indian Ocean. In the Northern Hemisphere, on the other hand, these changes indicate an intensification of both the Aleutian Low over the North Pacific Ocean and the Icelandic Low over the North Atlantic Ocean. In the Atlantic/European sector also the Azores High

is enhanced in the future, leading to an intensification of the North Atlantic Oscillation in the future. The reduction of the atmospheric pressure over the eastern tropical Pacific and the increase over the western part indicate an intensification of the Southern Oscillation in response to the El Niño-like warming pattern (see Fig 10a).

Again, in 2C20 (Fig. 12b) the future changes in the sea-level pressure have a similar structure as in A1B but with a reduction of the magnitude by about 50%. The change in the European region is, however, particularly strong with an intensification of the Azores High by up to 1.5 hPa compared to 2.0 hPa in A1B and a slightly weaker reduction of the atmospheric pressure over the Barents Sea and the Kara Sea. The changes in the Southern Hemisphere mid- and high latitudes, on the other hand, are rather weak in 2C20, with a relatively weak increase in the mid-latitudes as well as a rather weak decrease in the Antarctic region. This is clearly visible in the distribution of the differences between A1B and 2C20 (Fig. 12c), as the differences in the Southern Hemisphere mid- and high latitudes are enhanced by a factor of 2 to 3 compared to the future changes simulated in 2C20.

In contrast to the near-surface temperatures and precipitation, the effect of the higher aerosol emissions on the sea-level pressure does not have the same general structure as the effect of the increased greenhouse gas emissions. Significant differences between 2C30 and 2C30A (Fig. 12d) are pretty much localized, and have in some cases, i.e., south of Australia and south of Alaska, the same sign as the changes due to global warming. In other cases, i.e., in North Africa and western Europe, they can alter the climate change signal. Here, the higher aerosol emissions cause a southward shift of the Azores High (note that Fig. 12d shows the effect of the lower aerosol emissions).

## 5.5 Root-mean-square differences

Variable	$A1B_{fut} - A1B_{pre}$	$2C20_{fut} - A1B_{pre}$	$A1B_{fut} - 2C20_{fut}$	$2C30_{fut} - A1B_{pre}$	$2C30A_{fut} - A1B_{pre}$	$2C30_{fut} - 2C30A_{fut}$
Temperature in 2 m [°C]	3.46	1.81	1.69	2.02	1.45	0.60
Precipitation [mm/d]	0.54	0.27	0.39	0.33	0.27	0.28
Sea-level pressure [hPa]	1.55	0.62	1.02	0.73	0.63	0.30

**Table 3:** Rms differences of future changes for different experiments (A1B, 2C20, 2C30, and 2C30A) and between certain experiments (A1B vs. 2C20 and 2C30 vs. 2C30A). The periods considered are 1961-1990 (“pre”) and 2171-2100 (“fut”).

In order to get a general overview, the root-mean-square (“rms”) differences of the future climatic change in the different simulations (A1B, 2C20, 2C30, and 2C30A) as well as for the differences between A1B and 2C20 and between 2C30 and 2C30A for the future climate have been computed for the meteorological variables presented previously (Table 3).

As for the near-surface temperature, the rms differences follow the future changes in the global mean values (see Table 1) with the largest rms difference of 3.46 °C for A1B and the smallest value (1.45 °C) for 2C30A. While for the near-surface temperature the climatic change in 2C20 (1.81 °C) is stronger than the difference between A1B and 2C20 for the future climate (1.60 °C), the opposite is true for daily precipitation (0.27 vs. 0.39 mm/d) and sea-level pressure (0.62 vs. 1.02 hPa).

Apparently, despite the larger temperature differences, for these two meteorological variables the future climatic changes in 2C20 are generally weaker than the corresponding differences between A1B and 2C20 for the simulations of the future climate. The differences between 2C30 and 2C30A for the future climate are generally larger than the climatic changes simulated in 2C30A for the near-surface temperature (1.45 vs. 0.60 °C) and sea-level pressure (0.63 vs. 0.30 hPa), while the respective rms differences are about the same for precipitation (0.27 vs. 0.28 mm/d).

## 6. Summary and conclusions

The purpose of this study is to specify a particular scenario for keeping the future warming at 2 °C relative to pre-industrial levels, using the ECHAM5/MPI-OM coupled climate model. This scenario considers atmospheric greenhouse gas concentrations and anthropogenic aerosol emissions as well as ozone levels throughout the atmosphere. The projected changes in various meteorological and oceanic variables associated with this so-called “2 °C-stabilization” scenario are presented and compared to the respective changes associated with the SRES A1B scenario used in the upcoming IPCC-report. Furthermore, the role of the anthropogenic aerosol emissions for defining the stabilization scenario and their impact on the simulated future climate are investigated.

The 2 °C-stabilization scenario is characterized by the following atmospheric concentrations of the well-mixed greenhouse gases: 418 ppm (CO<sub>2</sub>), 2026 ppb (CH<sub>4</sub>), and 331 ppb (N<sub>2</sub>O), respectively, resulting in an equivalent CO<sub>2</sub> level of 488.6 ppm. These greenhouse gas concentrations correspond to the year 2020 according to the SRES A1B scenario (Nakićenović et al. 2000). At the same time, the anthropogenic aerosol emissions and the atmospheric ozone concentrations are changed to the level of 2100, again according to the A1B scenario. As for the SO<sub>2</sub>-emissions, this means a reduction from 92 TgS/yr in 2020 to 26 TgS/yr, while the ozone levels are somewhat higher than in 2020, i.e., by about 25% in the middle stratosphere. By this, the proposed equivalent CO<sub>2</sub> concentration is considerably smaller than the 550 ppm the European Union is aiming at as a stabilization level. At the same time, however, it is higher than the 400 ppm proposed by Meinshausen (2006) but close to the 475 ppm that according to Meinshausen (2006) are not very likely to keep the future warming below 2 °C. The latter suggests that the climate sensitivity of a complex coupled climate model is lower than the estimates of the climate sensitivities based on less complex models used in that study due to the inclusion of certain feedback mechanisms.

Although the simulation applying the 2 °C-stabilization scenario after 2020 (“2C20”) is stable throughout much of the 22<sup>nd</sup> century, it could be possible that at some later point in time the global mean temperature decreases again before reaching its equilibrium. This would, however, allow for a higher level of atmospheric greenhouse gas concentrations in order to keep the future warming below or at 2 °C beyond the 22<sup>nd</sup> century.

The magnitude of the future warming simulated in the different experiments strongly depends on the strength of the anthropogenic forcing. The simulation applying the A1B scenario until 2100 (“A1B”) gives an increase in the global mean temperature of 3.47 °C by the end of the 21<sup>st</sup> century compared to the warming of 1.92 °C in 2C20. Due to the unrealized warming, A1B shows a warming of 4.71 °C by the end of the 22<sup>nd</sup> century, while in 2C20 the future warming only slightly increases to 2.02 °C. The two other simulations with constant greenhouse gas concentrations after 2030 but different anthropogenic aerosol emissions (“2C30” and “2C30A”, respectively) give an increase in the global mean temperature of 2.13 °C (2C30) and 1.60 °C (2C30A) by the end of the 21<sup>st</sup> century. Correspondingly, the magnitudes of the future changes in the global mean precipitation and in the sea-ice conditions in the Arctic and the Antarctic region, respectively, differ between the different simulations. However, 2C30 and 2C30A give the same magnitude for the future changes in sea-ice conditions in the Antarctic region. The different simulations also show that the time that the simulation needs to reach its equilibrium after the anthropogenic forcing is kept constant

strongly depends on the magnitude of the future warming. While the simulations aiming at a future warming of 2 °C are close to their equilibrium after 50-60 years, A1B has not reached its equilibrium after 100 years of simulation, in particularly regarding the sea-ice conditions.

The local changes in the future climate simulated in the four different experiments show generally the same patterns, i.e., a pronounced temperature increase, in particular in the high latitudes accompanied by a marked reduction of the sea-ice cover, a substantial increase in precipitation in the tropics and in the mid- and high latitudes of both hemispheres but a marked reduction in the subtropics, and a significant strengthening of the meridional pressure gradient in the extratropics accompanied by a pronounced intensification of the jet streams in the upper troposphere. The magnitude of these changes, however, strongly depends on the magnitude of the anthropogenic forcing, with A1B giving the strongest changes and 2C30A the weakest. By the end of the 21<sup>st</sup> century the changes simulated in 2C20, for instance, are generally less than half as strong as the changes associated with the A1B scenario. Hence, the differences between these two scenarios generally exceed the future changes associated with the 2 °C-stabilization scenario. This does, however, not mean that the changes simulated in 2C20 are small. The annual mean near-surface temperatures in the Arctic region, for instance, are expected to increase by 4-5 °C, over the Barents Sea by up to 7 °C going along with a substantial reduction of the sea-ice in this area in all seasons. Over the North Atlantic, the meridional pressure gradient is increased by about 4 hPa, resulting in a higher storm activity over the eastern North Atlantic and Europe. In the Southern Hemisphere subtropics, on the other hand, annual mean precipitation is reduced by about 0.15 mm/d in the zonal mean, corresponding to 10% of the present-day values, increasing the risk of droughts in these regions.

The higher anthropogenic aerosol emissions in 2C30A generally weaken the future changes in climate related to both the direct and the indirect effect of sulphate aerosols. Since the main sources for anthropogenic aerosol emissions are located in the industrialized areas, the effects are most pronounced in the Northern Hemisphere and in the tropics. In the Arctic region, for instance, the future warming is about 1 °C weaker and the meridional pressure gradient over the North Atlantic is 1 hPa weaker. In particular the future changes in precipitation are affected by the higher aerosol emissions, with a significantly weaker increase in the annual mean precipitation in the tropics and in the Northern Hemisphere extratropics, with zonal mean differences of about 0.15 mm/d in the tropics and up to 0.10 mm/d in the Northern Hemisphere extratropics.

In order to investigate to which extent the choice of the year after which the greenhouse gas concentrations have to be kept constant so that the global mean temperature does not exceed 2.0 °C by the end of the 21<sup>st</sup> century depends on the climatic state, an additional simulation similar to 2C20 has been performed. In this simulation, referred to as “2C20M”, the atmospheric concentrations of the greenhouse gases and ozone as well as the aerosol emissions are prescribed as in 2C20 but the simulation was started from a different climatic state originating from a simulation performed at the Max-Planck-Institute for Meteorology (“MPI”) in Hamburg corresponding to A1B. According to Fig. 13a, 2C20M is colder than 2C20 for about 50 years, reaching the same change in temperature at about 2060. One reason for this is the colder climate state of the simulation provided by MPI, the other is the relatively weak warming during the first 10 years of 2C20M (Fig. 13b). The warming of more than 0.5 °C/century continues about 10 years longer in 2C20M, leading to the same temperature change at about 2060. Also after about 2060, variations at decadal time scales give rise to small differences between 2C20M and 2C20, resulting in a warming of 1.88 °C by the end of the 21<sup>st</sup> century in 2C20M and 1.92 °C in 2C20 (see Table 2). Also, 2C20M exceeds the threshold of 2 °C about 20 years later than 2C20. It is interesting to note that, in contrast to 2C20, 2C20M has not yet reached its equilibrium by the end of the 22<sup>nd</sup> century but continues to warm slightly. As a consequence, 2C20M reaches a slightly stronger warming of 2.06° as compared to 2.02 °C by the end of the 22<sup>nd</sup> century.

## Near-surface temperature

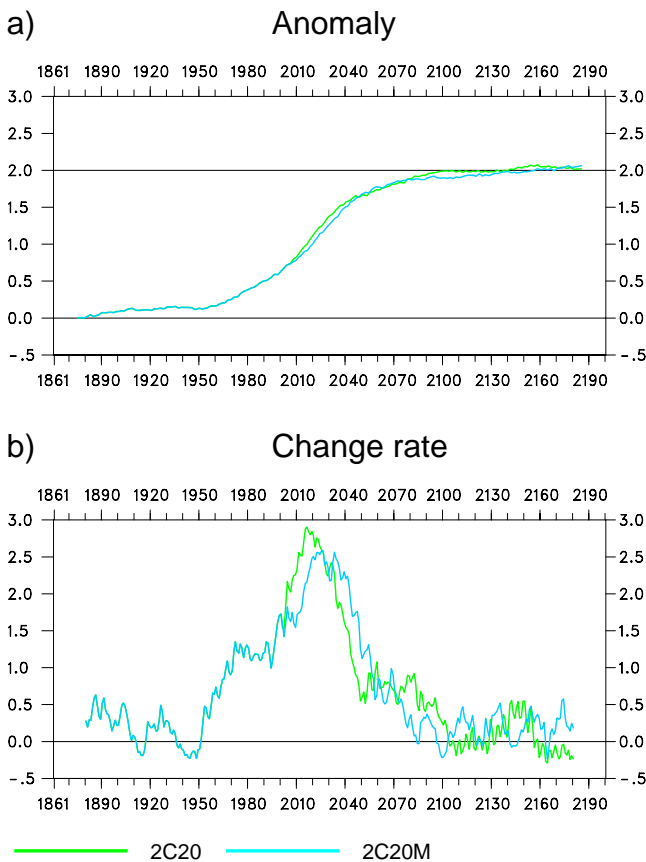


**Figure 13:** As Fig. 1, but for 2C20 and a corresponding simulation starting from a different climate state (“2C20M”).

The choice of the particular greenhouse gas concentrations at which the future warming does not exceed the threshold of 2 °C depends on the climate sensitivity of the coupled model. A climate model with a higher sensitivity would require weaker greenhouse gas concentrations and a model with a lower sensitivity would allow for higher concentrations and, hence, for a later time at which the greenhouse gas concentrations have to be kept constant. Since ECHAM5/MPI-OM’s climate sensitivity is neither very low nor a very high compared to other climate models, the estimate presented here could be a quite realistic recommendation for a 2 °C-stabilization scenario.

This study also illustrates the difficulties in defining a particular scenario on the basis of a particular value of the future warming using a particular coupled climate model, especially to the different climate sensitivity of different climate models but also due to climate variations on decadal time scales. More fruitful might be an approach similar to the approach used in the IPCC-report, i.e., to define particular “2 °C-scenarios” that one would expect to give a future warming of about 2 °C and then perform a number of simulations with several different climate models using several 2 °C-scenarios. These scenarios should be based on different assumptions regarding socio-economic, technological and demographic developments, such as those used in the IPCC-report (Nakićenović et al. 2000). Especially, these scenarios could include more realistic temporal evolutions of the greenhouse gas concentrations rather than keeping them at a constant level at a particular point in time. This approach would, in contrast to this study, allow for an estimate of the probability that the future warming actually could be kept at 2 °C under certain assumptions.



The atmospheric concentrations of greenhouse gases such as CO<sub>2</sub> and CH<sub>4</sub> can undergo pronounced changes due to exchanges with the oceans or the land-surface is association with a variety of different processes. Hence, these interactions effect the long-term development of the earth's climate and ideally should be included in the construction of a stabilization scenario. This would, however, require more complex climate models, including, for example, fully coupled carbon or methane cycles as well as interactive vegetation.

## **Acknowledgements**

This work was supported by the Danish Environmental Protection Agency and the European Commission through the ENSEMBLES project under contract no. GOCE-CT-2003-505539.

## References

- ACIA (2005) Arctic Climate Impact Assessment. Cambridge University Press, Cambridge, UK, pp 1042
- Archer D, Martin P, Buffett B, Brovkin V, Rahmsdorf S, Ganopolski A (2004) The importance of ocean temperature to biogeochemistry. *Earth Planet Science Letts* 222: 333-348
- Boucher O, Lohmann U (1995) The sulphate-CCN-cloud albedo effect: A sensitivity study using two general circulation models. *Tellus* 47B: 281-300
- Brasseur GP, Roeckner E (2005) Impact of improved air quality on the future evolution of climate. *Geophys Res Lett* 32: 10.1029/2005GL023902
- Buffett B, Archer D (2004) Global inventory of methane clathrate: Sensitivity to changes in the deep ocean. *Earth Planet Science Letts* 227: 185-199
- Cubasch U, 8 co-authors (2001) Projections of future climate change. In: Houghton JT, Ding Y, Griggs DJ, Noguer M, van der Linden PJ, Dai X, Maskell K, Johnson CS (eds), *Climate Change 2001. The scientific basis*. Cambridge University Press, Cambridge, UK, 525-582
- Den Elzen M, Meinshausen M (2006) Multi-gas emission pathways for meeting the EU 2°C climate target. In: Schellnhuber HJ, Cramer W, Nakićenović NJ, Wigley T, Yohe G (eds) *Avoiding Dangerous Climate Change*. Cambridge University Press, Cambridge, UK, 299-309
- Friedlingstein P, Dufresne JJ, Cox PM, Rayner P (2003) How positive is the feedback between climate change and the carbon cycle? *Tellus* 55B: 692-700
- Gregory JM, Huybrechts P, Raper SCB (2004) Climatology: Threatened loss of the Greenland ice-sheet. *Nature* 428: 616
- Hess M, Koepke P, Schult I (1998) Optical properties of aerosols and clouds: The software package OPAC. *Bull Amer Meteorol Soc* 79: 831-844
- Huybrechts P, Letreguilly A, Reeh A (1991) The Greenland ice-sheet and global warming. *Glob Planet Change* 89: 399-412
- Houghton JT, Ding Y, Griggs DJ, Noguer M, van der Linden PJ, Dai X, Maskell K, Johnson CS (eds) (2001) *Climate Change 2001. The scientific basis*. Cambridge University Press, Cambridge, UK, pp 881
- Jones CD, Cox P, Essery RLH, Roberts DL, Woodage MJ (2003a) Strong carbon cycle feedbacks in a climate model with interactive CO<sub>2</sub> and sulphate aerosols. *Geophys Res Letts* 30: 1479-1483
- Jones CD, Cox P, Huntingford C (2003b) Uncertainty in climate-carbon-cycle projections associated with the sensitivity of soil respiration to temperature. *Tellus* 55B: 642-648
- Jungclaus JH, Botzet M, Haak H, Keenlyside N, Luo JJ, Latif M, Marotzke J, Mikolajewicz U, Roeckner E (2006) Ocean circulation and tropical variability in the coupled model ECHAM5/MPI-OM. *J Clim* 19: 3952-3972
- Marsland SJ, Haak H, Jungclaus JH, Latif M, Röske F (1998) The Max-Planck-Institute global ocean/sea ice model with orthogonal curvilinear coordinates. *Ocean Modell* 5: 91-127
- Meinshausen M (2006) What does a 2°C target mean for greenhouse gas concentrations? A brief analysis based on multi-gas emission pathways and several climate sensitivity uncertainty estimates. In: Schellnhuber HJ, Cramer W, Nakićenović NJ, Wigley T, Yohe G (eds) *Avoiding Dangerous Climate Change*. Cambridge University Press, Cambridge, UK, 265-279
- Nakićenović NJ, 27 co-authors (2000) IPCC special report on emission scenarios. Cambridge



University Press, Cambridge, UK, pp 599

Roeckner E, 13 co-authors (2003) The atmospheric general circulation model ECHAM5. Part I: Model description. MPI-Report 349: pp 127

Roeckner E, Brokopf R, Esch M, Giorgetta M, Hagemann S, Kornblüh L, Manzini E, Schlese U, Schulzweida U (2006) Sensitivity of simulated climate to horizontal and vertical resolution in the ECHAM5 atmosphere model. J Clim 19: 3771-3791

Schellnhuber HJ, Cramer W, Nakićenović NJ, Wigley T, Yohe G (eds) (2006) Avoiding Dangerous Climate Change. Cambridge University Press, Cambridge, UK, pp 392

Smith JB, Schellnhuber HJ, Mirza MQM (2001) Vulnerability to climate change and reasons for concern: A synthesis. In: McCarthy JJ, Canziani OF, Leary NA, Dokken DJ, White KS (eds), Climate Change 2001. Impacts, Adaptation, and Vulnerability. Cambridge University Press, Cambridge, UK, 913-967

United Nations (1992) United Nations Framework Convention on Climate Change (UNFCCC). Available at <http://www.unfccc.int>

Wigley TML, Raper SCB (2001) Interpretation of high projections for global-mean warming. Science 293: 451-454

## Previous reports

Previous reports from the Danish Meteorological Institute can be found on:  
<http://www.dmi.dk/dmi/dmi-publikationer.htm>